

Impact of present and future aircraft NO_x and aerosol emissions on atmospheric composition and associated direct radiative forcing of climate

5 Etienne Terrenoire^{1,2}, Didier A. Hauglustaine¹, Yann Cohen¹, Anne Cozic¹, Richard Valorso³,
Franck Lefèvre⁴, and Sigrun Matthes⁵

¹Laboratoire des Sciences du Climat et de l'Environnement (LSCE), UMR 8212, Gif-sur-Yvette, France.

²Now at Office National d'Etudes et de Recherches Aéronautiques (ONERA), DMPE, Université Paris-Saclay, Palaiseau, France.

³Univ. Paris-Est-Créteil and Univ. Paris Cité, CNRS, LISA, F-94010 Créteil, France.

10 ⁴Laboratoire Atmosphères, Milieux, Observations Spatiales (LATMOS), UMR 8190, Paris, France.

⁵Deutsches Zentrum für Luft-und Raumfahrt e.V., DLR Institut für Physik der Atmosphäre, Oberpfaffenhofen, 82334 Wessling, Germany

Correspondence to: D. A. Hauglustaine (didier.hauglustaine@lsce.ipsl.fr)

15 **Abstract.**

15

Aviation NO_x emissions have not only an impact on global climate by changing ozone and methane levels but also contribute to deteriorate local air quality. A new version of the LMDZ-INCA global model, including both tropospheric and stratospheric chemistry and the sulfate-nitrate-ammonium cycle, is applied to re-evaluate the impact of aircraft NO_x and aerosol emissions on climate. The results confirm that the efficiency of NO_x to produce ozone is very much dependent on the injection height and increases with the background methane and NO_x concentrations and with decreasing aircraft NO_x emissions. The methane lifetime variation is less sensitive to the aircraft NO_x emission location than the ozone change. The net NO_x radiative forcing (O₃ + CH₄) is largely affected by the revised CH₄ radiative forcing formula. The ozone positive forcing and the methane negative forcing largely offset each other resulting in a slightly positive forcing for the present-day. However, in the future, the net forcing turns to negative due essentially to higher methane background concentrations. Additional radiative forcings involving particle formation arise from aircraft NO_x emissions since the increased OH concentrations are responsible for an enhanced conversion of SO₂ to sulfate particles. Aircraft NO_x emissions also increase the formation of nitrate particles in the lower troposphere. However, in the upper-troposphere, increased sulfate concentrations favor the titration of ammonia leading to lower ammonium nitrate concentrations. The climate forcing of aircraft NO_x emissions is likely to be small or even switch to negative (cooling) depending on atmospheric NO_x or CH₄ future background concentrations or when the NO_x impact on sulfate and nitrate particles is considered. However, there remain large uncertainties on the NO_x net impact on climate and in particular on the indirect forcings associated with aerosols which are even more uncertain than the other forcings from gaseous species. Additional studies with a range of models are hence needed in order to provide a more consolidated view. Nevertheless, our results suggest that reducing aircraft NO_x emissions is primarily beneficial for improving air quality.

20
25
30
35

1 Introduction

40 Air traffic emissions represent a sizeable contribution to global anthropogenic climate change (Lee et al., 2021) and also to regional surface air pollution, in particular around airports (Yim et al., 2015). Aircraft release in the atmosphere not only gaseous compounds such as carbon dioxide (CO₂), nitrogen oxides (NO_x), hydrocarbons (HC), sulfur dioxide (SO₂) and water vapour (H₂O), but also particulate material composed of ice crystals, soot particles (Black Carbon, BC) and sulfates (SO₄) (e.g., Kärcher, 2018; Lee et al., 2021). There is a wide range of
45 spatial and temporal scales associated with atmospheric perturbations due to aircraft emissions. It ranges from the local and plume scales for chemical species, aerosols, and contrail-cirrus formation to the global scale for methane and carbon dioxide perturbations; and from a few minutes after emission up to several decades (Brasseur et al., 2016). Evaluating the global chemical and climate perturbations associated with aircraft emissions therefore appears as a complex issue.

50 Due to this range of scales and also to the different nature of the perturbations of the climate system involved, a distinction is usually made between the CO₂ and the non-CO₂ climate impacts of aviation. These climate forcings were recently reassessed by Lee et al. (2021). For 2018, the net aviation Effective Radiative Forcing (ERF) of historic aviation emissions until 2018 was estimated in this recent study to 101 mW/m² with major contributions
55 from contrail cirrus (57.4 mW/m² or 57% of the total forcing), CO₂ (34.3 mW/m², 34%), and NO_x (17.5 mW/m², 17%). Non-CO₂ terms represent a net positive forcing that accounts for more than half (66%) of the aviation total radiative forcing of climate. In contrast to the CO₂ forcing which is relatively well determined except for some methodological issues (Terrenoire et al., 2019; Ivanovich et al., 2019; Boucher et al., 2021), non-CO₂ forcing terms contribute about 8 times more than CO₂ to the uncertainty in the aviation total forcing (Lee et al., 2021).

60 From these non-CO₂ climate forcings associated with aircraft emissions, nitrogen oxides (NO_x) play a particular role. Indeed, not only do they affect climate by changing the atmospheric concentration of ozone (O₃) and methane (CH₄) (e.g., Hauglustaine et al., 1994; Brasseur et al., 1998; Holmes et al., 2011; Myhre et al., 2011), two important greenhouse gases, but they also have an impact on local air quality and human health, both through emissions in
65 and around airports and from emissions at higher altitude affecting near-ground background concentrations (e.g., Barrett et al., 2010; Hauglustaine and Koffi, 2012; Cameron et al., 2017). For this reason, it has been assumed that emissions standards for NO_x emissions set since the 1980s by the International Civil Aviation Organization (ICAO) were not only protecting local air quality but also had co-benefits for climate change mitigation (Skowron et al., 2021). A technological difficulty faced by aircraft industry today is that reducing NO_x emissions tends to
70 increase fuel burn, hence resulting in increased CO₂ emissions and a climate penalty (Freeman et al., 2018). There is however a possibility that technological development could lead simultaneously to CO₂ and NO_x emissions reduction (Prashanth et al., 2021). Hence, a better quantification of the aircraft NO_x effect on climate is needed to determinate if the climate effect of CO₂ increase linked to new technology could be compensated by the associated NO_x reduction.

75 Emissions of NO_x into the troposphere result in a short-term increased photochemical ozone production (resulting in a positive climate forcing or warming), and a long-term increased oxidation of atmospheric methane through reaction with the hydroxyl radical (OH) (resulting in a negative climate forcing or cooling), as shown by Fuglestvedt et al. (1999) and Naik et al. (2022). In addition, the aforementioned methane reduction results in a
80 long-term reduction in tropospheric O₃ (cooling) and a long-term reduction in H₂O in the stratosphere (cooling). In the lower troposphere, the net effect of NO_x emissions is dominated by the increased methane destruction and a negative forcing is predicted. In the upper-troposphere, at aircraft cruise altitudes, the ozone production is about 5 times more efficient per molecule of NO_x emitted (e.g., Hauglustaine et al., 1994; Derwent et al., 2001; Hoor et al., 2009; Dahlmann et al., 2011) and a positive net radiative forcing of climate is generally associated with aircraft
85 NO_x emissions (e.g., Holmes et al., 2011; Myhre et al., 2011; Hoor et al., 2009; Søvde et al., 2014; Brasseur et al., 2016; Lee et al., 2021). Based on an in-depth literature assessment, Lee et al. (2021) provided the most recent estimate of these forcings and derived a net NO_x radiative forcing from all emissions released by aviation of 17.5 (0.6, 28.5) mW/m² in 2018, decomposed into a positive short-term tropospheric ozone forcing of 49.3 (32, 76) mW/m² and a negative methane forcing of -34.9 (-65, -25.5) mW/m². The aircraft NO_x net radiative forcing of
90 climate is positive but this net effect is the sum of two forcings of opposite sign, distinct geographic distributions and each of them associated with large uncertainties.

95 Recently, Skowron et al. (2021) reinvestigated the aircraft NO_x climate forcing based on various future scenarios for both surface and aircraft NO_x emissions using the MOZART-3 global chemistry-climate model (Kinnison et al., 2007). They found that in all their future (2050) simulations and even for “present-day” (2006) simulations under certain conditions, the net radiative forcing from aircraft NO_x could turn negative. This finding is essentially associated with the revised expression for methane direct radiative forcing from Etminan et al. (2016) which increases, for instance, the methane forcing by 24.5 % for a halving of its atmospheric concentration compared to previous formulations. However, another major uncertainty associated with the impact of NO_x emissions on
100 atmospheric composition arises from the non-linear character of the tropospheric chemistry. This feature makes the impact of aircraft NO_x dependent on the background atmospheric concentrations and hence sensitive to anthropogenic surface emissions of NO_x, CO and hydrocarbons or even to natural emissions such as lightning NO_x (Holmes et al., 2011; Skowron et al., 2021). It also makes the impact of aircraft NO_x very dependent on the location

105 of the emission and on the season (Stevenson et al., 2004; Stevenson and Derwent, 2009; Gilmore et al., 2013; Skowron et al., 2013; Søvdde et al., 2014). Since the ozone production sensitivity differs from the methane destruction sensitivity, the positive short-term ozone forcing associated with aircraft NO_x can be overwhelmed by the methane negative forcing, providing a negative net radiative forcing of climate (Stevenson and Derwent, 2009; Skowron et al., 2021).

110 Other effects of aircraft NO_x emissions, less accounted for in earlier studies, include the role played by tropospheric aerosols and in particular the impact on secondary inorganic aerosols such as nitrates and sulfates (Unger, 2011; Pitari et al., 2015; Brasseur et al., 2016; Lund et al., 2017; Prashanth et al., 2022). Increased NO_x emissions from aircraft have indeed the potential to form ammonium nitrates particles. However, the changes in oxidants and the direct emission of SO₂ by aircraft also increase the formation of sulfate particles with possible implications on
115 nitrate concentrations (Unger et al., 2013; Righi et al., 2013; 2016). These indirect forcings associated with aircraft NO_x emissions are however complex and need further investigation since they can provide additional negative direct forcings of climate. In order to account for the role played by secondary inorganic aerosols and other interactions involving gas-phase and aerosols chemistry, the global models used to assess the impact of aircraft NO_x emissions need to include both gas phase chemistry, tropospheric aerosols and in particular the role played
120 by the sulfate-nitrate-ammonium cycle.

The aim of the present study is to provide a comprehensive and updated model-based analysis of the impact of aircraft NO_x emissions on atmospheric composition and associated radiative forcing of climate. The LMDZ-INCA global model, including both tropospheric and stratospheric chemistry as well as tropospheric aerosols, is applied.
125 An earlier and less mature version of this model has been previously used by Koffi et al. (2010) and Hauglustaine and Koffi (2012), or in several model intercomparisons (Hoor et al., 2009; Hodnebrog et al., 2011; 2012; Myhre et al., 2011) in order to investigate the impact of NO_x transport emissions on atmospheric composition and climate. This earlier version of the model only included tropospheric gas phase chemistry and used a coarser vertical resolution. The new version of LMDZ-INCA used in this study allows us to revisit the impact of aircraft NO_x on ozone production, changes in oxidants and methane destruction but also the impact on the secondary inorganic aerosol distributions. These earlier studies will provide a point of comparison for this new assessment. This study focuses on the effect of aircraft NO_x emissions but also includes aircraft SO₂ and aerosols emissions in order to account for the effect of the sulfate-nitrate-ammonium cycle and consider the potential effect linked to heterogeneous chemistry. Similarly, the direct water vapour aircraft emission is also included in order to account
130 for the role of stratospheric water vapour on atmospheric oxidants and in link also with the methane indirect effect on H₂O.
135

Moreover, another aim of this paper is to investigate the sensitivity of the aircraft NO_x net radiative forcing of climate to various mitigation options. Motivated by earlier work (e.g., Unger, 2011; Hodnebrog et al., 2012; Matthes et al., 2021; Skowron et al., 2021) we assess in particular the sensitivity of the NO_x forcing to a variation of the aircraft emission injection height and to background (present versus future) atmospheric concentrations. In the future, several scenarios are considered in order to investigate low and high assumptions in air-traffic growth and fuel burn efficiencies. Other scenarios will also illustrate more specifically the impact of desulfurized jet fuel as a mitigation option or engines with ultra-low NO_x combustor technology. For all these “present-day” and future
140 (2050) scenarios, the changes in atmospheric composition are illustrated and the radiative forcings of climate associated with NO_x emissions (O₃ and CH₄ direct and indirect forcings) and with aerosol direct effects are calculated.
145

The remainder of this paper is organized as follows. In **Section 2**, we present the aircraft emission inventories prepared and introduced in the global chemistry-climate model for both the “present-day” baseline simulation and for the future (2050) baseline and mitigation scenarios. In **Section 3**, we provide a description of the LMDZ-INCA chemistry-climate model used in this study along with a description of the radiative forcing calculations and modelling set-up. In addition, in **Section 3**, we also summarize the model performance comparing the model results with ozone soundings and with the IAGOS (In-service Aircraft for a Global Observing System) measurements of ozone and carbon monoxide concentrations in the upper-troposphere and lower-stratosphere. In
150 **Section 4**, we present the atmospheric composition perturbations associated with the “present-day” aircraft emissions and in **Section 5** the perturbations associated with future aircraft emissions under different scenarios. We then present the radiative forcings of climate associated with the changes in atmospheric composition in **Section 6**. Finally, in **Section 7**, we discuss conclusions drawn from this study.
155
160

2 Aircraft emissions

The global three-dimensional and time varying aircraft emission inventories used in this study are essentially based on the previous Reducing Emissions from Aviation by Changing Trajectories for the benefit of Climate (REACT4C) (Matthes et al., 2012) and Quantifying the Climate Impact of Global and European Transport Systems (QUANTIFY) (Lee et al., 2010) European Union (EU) projects. These inventories are based on the fuel-flow model PIANO (Project Interactive Analysis and Optimization model) and the global emission model FAST (Future Aviation Scenario Tool) with air traffic movements coming from radar data for flights for Europe and North America and the the Official Airline Guide (OAG) database for the remaining global flight movements (Lee et al.,
165

170 2009; Owen et al., 2010). For this specific study, the methodology used to derive emissions for the global
chemistry-transport model LMDZ-INCA is further described in the following Section 2.1 for “present-day”
baseline emissions and in Section 2.2 for the future (2050) emission scenarios.

175 2.1 “Present-day” baseline emissions

175 The aircraft emission inventory used for “present-day” baseline emissions is based on the EU project REACT4C
(Matthes et al., 2012, 2021; Søvde et al., 2014; Grewe et al., 2014) and is representative of the year 2006. This
inventory will be referred to as REACT4C_2006 in this paper. The REACT4C_2006 data includes three-
180 dimensional gridded distributions of travelled-km, fuel consumption, as well as CO₂, NO₂, and BC (Black Carbon,
soot) emissions. Flight data are derived from CAEP8 data using the “great circle distance” method corrected with
the CAEP8 formula. This dataset is available on a latitude-longitude-altitude grid for 12 months with a horizontal
resolution of 1°x1° and a 610 m vertical resolution. In this inventory, the global mean NO_x Emission Index (EI) is
12.1 gNO₂/kg fuel (12.7 gNO₂/kg below 1800 m and 12.3 gNO₂/kg above 8400 m). For BC, the mean EI is 0.023
185 gBC/kg fuel (0.046 gBC/kg below 1800 m and 0.015 gBC/kg above 8400 m). Additional species are needed to
run the global chemistry-transport model. For H₂O, carbon monoxide (CO) and total non-methane hydrocarbons
(HC), we use the three-dimensional emissions from the AERO2K project inventory (Eyers et al, 2005). The EIs
for these species are derived for the AERO2K vertical levels (500 feet vertical resolution) and interpolated onto
the REACT4C vertical levels. Based on the REACT4C fuel burn we then derive the H₂O, CO and HC three-
dimensional and monthly emissions representative of the year 2006. For HC we use the speciation given by FAA
190 (2009) in order to derive the emissions of the LMDZ-INCA model individual hydrocarbons. For Organic Carbon
(OC), SO₂ and SO₄, we use the mean EIs reported by Lee et al. (2010). For OC, Lee et al. (2010) provide a range
of 0.0065-0.05 g/kg. As was done by Balkanski et al. (2010) and Righi et al. (2016), we choose the highest EI
value of 0.05 g/kg fuel and determine a maximum value for organic carbon produced from aircraft. For SO₂ and
SO₄, the mean EIs are respectively 0.8 and 0.04 g/kg fuel. From REACT4C_2006, we derive global EIs of 3.15
195 kgCO₂/kg fuel, 1.23 kgH₂O/kg fuel, 3.25 gCO/kg fuel, and 0.405 gHC/kg fuel, which compares well to the EI_{CO₂}
and EI_{H₂O} used in Lee et al. (2021) recent review. They are somewhat lower than the EIs used in Lee et al. (2021)
for BC (EI_{BC}=0.03 gBC/kg fuel), NO_x (EI_{NO_x}=14.12 gNO₂/kg fuel) and SO₂ (EI_{SO₂}=1.2 g/kgfuel). **Table 1**
summarizes the total emissions for the baseline REACT4C_2006 inventory. **Figure S1** shows the zonal and annual
mean distribution of REACT4C_2006 fuel use, NO₂ and BC emissions.

200 The REACT4C_2006 inventory is chosen for the “present-day” baseline simulation since this inventory provides,
in addition to the baseline emissions, two additional mitigation inventories. These mitigation scenarios based on
the original REACT4C_2006 emissions were used in this study in order to investigate the sensitivity of the
chemical perturbations and associated radiative forcings to a cruise altitude variation (Søvde et al., 2014, Matthes
205 et al., 2021). REACT4C_PLUS corresponds to the original REACT4C_2006 inventory with flight altitude
increased by 2000 feet (610 m) while in REACT4C_MINUS the flight altitudes been decreased by 2000 feet.
While the total distance flown is approximately equal in all REACT4C inventories, as fuel efficiency increases
with altitude, the fuel use is 178, 177 and 181 Tg/yr in the baseline, REACT4C_PLUS and REACT4C_MINUS
inventories, respectively. As a consequence, the total NO_x emissions are respectively 0.71, 0.72 and 0.71 TgN/yr.

210 In order to compare the future perturbations based on the QUANTIFY project emissions (see next section) to the
“present-day” perturbations, another reference inventory has been used in this paper. This inventory labelled
QUANTIFY_2000 is based on the QUANTIFY assumptions as described in Owen et al. (2010). In particular, this
QUANTIFY_2000 reference is scaled based on IEA sales justifying the higher fuel burn compared to
215 REACT4C_2006. The QUANTIFY emission inventory has been extended to the additional species needed in the
global chemistry-transport model as described above. As a consequence of the 20% higher fuel consumption and
different assumptions for EIs (for BC and NO_x) in this inventory, the total emissions of primary species are higher
by 18-25% than those provided for REACT4C_2006 (**Table 1**). This inventory is only used for the sake of
comparison with the more recent REACT4C_2006 inventory and as baseline for the future perturbations for which
220 2050 QUANTIFY inventories are used.

Table S1 gives the total global emissions for the REACT4C_2006 and QUANTIFY_2000 inventories used in this
study and compares to the Aviation Climate Change Research Initiative (ACCRI) 2006 Aviation Environmental
225 Tool (AEDT) (Wilkerson et al., 2010; Brasseur et al., 2016) and Community Emissions Data System (CEDS)
2006 (Hoesly et al., 2018) inventories. The AEDT and CEDS inventories use the US governmental’s Volpe
National Transportation Systems Centre data. It should be noted that these inventories not only differ in terms of
total fuel use and global emissions but also in terms of vertical distributions as described in Skowron et al. (2013).
The QUANTIFY_2000 CO₂ emissions are close to the estimate of 686 TgCO₂/yr for 2000 provided by Lee et al.
(2021). In 2006, Lee et al. (2021) estimated an emission of 745 TgCO₂/yr, larger than the REACT4C_2006,
230 ACCRI and CEDS inventories by 33%, 25%, and 4%, respectively. Over the 2006-2018 period, Lee et al. (2021)
estimated an increase of 39%, reaching 1034 Tg CO₂/yr in 2018. The radiative forcings calculated with the
REACT4C_2006 inventory will be rescaled based on these CO₂ emissions for 2018 in order to be compared to the
forcings provided by Lee et al. (2021) at the end of this study.

235 2.2 Future 2050 emission scenarios

In this study, the future aircraft emission inventories prepared during the QUANTIFY EU project, and representative of the year 2050 are used (Owen et al., 2010). These scenarios were developed more than 10 years ago based on earlier economic assumptions regarding future Gross Domestic Product (GDP) growth and aviation demands in various regions according to the former IPCC Special Report on Emission Scenarios (SRES) storylines (Nakicenovic and Swart, 2000). These scenarios are still used in this study since they can be considered as benchmark scenarios, used in numerous former model simulations and intercomparisons (e.g., Koffi et al., 2010; Hodnebrog et al., 2011; 2012; Righi et al., 2016). These scenarios compare fairly well in terms of total future aircraft emissions to the more recent inventories. Three different aircraft emission inventories are selected in this study: the A1B (labelled QUANTIFY_A1 in the following), B1 (QUANTIFY_B1) and B1_ACARE (QUANTIFY_B1_ACARE) scenarios. These scenarios are described in details in Owen et al. (2010) and are only briefly summarized in the following. The scenario A1B is representative of an intense growth of the aviation sector during the first part of the century where global demand is driven by growth of the global economy. Due to technological improvements and introduction of new and less polluting airplanes within the overall fleet, the fuel efficiency improvement is assumed to be approximately 1% yr⁻¹ over the period 2000-2050. In contrast, the scenario B1 is a mitigation scenario in which the propensity to travel is reduced due to a goal to limit the environmental impact of aviation and to improve local air quality in particular. The fuel efficiency improves by 1% yr⁻¹ over the 2000-2020 period and increases by 1.3 % yr⁻¹ after 2020. This leads to a significant reduction of NO_x, SO₂ and BC global emissions in 2050 for this scenario. Finally, assuming the technology targets of the Advisory Council for Aeronautical Research in Europe (ACARE) in 2010, the alternative scenario B1_ACARE is an ambitious mitigation scenario which main goal is to limit the environmental impact of aviation. In this scenario the fuel efficiency assumptions are further tightened and the efficiency improves by 2.1% yr⁻¹ after 2020. As a result, the fuel consumption is divided by more than a factor 2 compared to the A1B scenario in 2050. The reduction hypotheses behind this extreme goal are the ACARE 2050 goals, which for example aim at a 40% improvement in aircraft fuel efficiency (with a further 10% improvement from air traffic management) compared to an equivalent new aircraft introduced in 2000. The variables available from the QUANTIFY three-dimensional inventories are the fuel burn, NO_x and BC emissions. The highest NO_x EIs derived from these inventories are for the A1B scenario and reaches 15.2 gNO₂/kg fuel (20 gNO₂/kg below 1800 m and 13.3 gNO₂/kg above 8400 m). For the mitigation scenarios B1 and B1_ACARE, the technology improvement strongly impacts the NO_x emissions and the EIs decrease by about a factor of 2 (i.e., 7.9 gNO₂/kg fuel and 7.3 gNO₂/kg fuel for B1 and B1_ACARE, respectively). For BC, the EI remains fairly constant in the various QUANTIFY future scenarios (0.022, 0.021 and 0.019 gBC/kg fuel for A1B, B1 and B1_ACARE, respectively). The EIs for other species (i.e. H₂O, CO, HC, OC, SO₂, SO₄) are assumed to be similar to those used for the REACT4C emission inventory.

In addition to the QUANTIFY A1, B1 and B1_ACARE scenarios, two other mitigation scenarios are used for the perturbation simulations. The QUANTIFY_LowNO_x scenario is identical to the A1 scenario with the NO₂ emission index divided by a factor of 2. This scenario is intended to illustrate one of the ACARE objectives of reducing NO_x emissions by the 2050 time-horizon compared to 2000. Similarly, the A1_Desulfurized scenario corresponds to the QUANTIFY_A1 scenario, with SO₂ and sulfate emissions imposed to 0 to illustrate the impact of desulfurized fuels on the chemical composition perturbations and climate. **Table 2** summarizes the total global emissions in 2050 for the different considered species and for the QUANTIFY_A1, QUANTIFY_B1 and QUANTIFY_B1_ACARE scenarios. As expected, for the QUANTIFY_A1 scenario, an increase in overall fuel consumption compared to the QUANTIFY_2000 of a factor of 3 is obtained and a factor 4 for NO_x. For the QUANTIFY_B1 and QUANTIFY_B1_ACARE scenarios the NO_x emissions are reduced by a factor of 3.3 and 4.8, respectively, compared to the A1B scenario. The BC emissions are reduced by a factor of 1.8 and 2.5, respectively, and the SO₂ emissions by a factor of 1.7 and 2.3 respectively. **Figure S1** compares the zonal and annual mean distribution of REACT4C_2006 and QUANTIFY_A1_2050 fuel use, NO₂ and BC emissions.

The total emissions from the QUANTIFY inventories are compared for 2050 to the recent Shared Socioeconomic Pathways (SSP) scenarios (Hoesly et al., 2018) and to the ACCRI AEDT scenarios (Brasseur et al., 2016) at **Table S2**. The ACCRI 2050-Base scenario is a high emission scenario providing emissions even higher than the QUANTIFY_A1 scenario, in particular in terms of BC emissions (81% higher emissions), SO₂ (87% higher) and to a lesser extent for NO_x (20% higher). We also note for comparison that Skowron et al. (2021) recently assumed a high air-traffic growth and low technology development reaching a high NO_x emission of 5.59 TgN yr⁻¹ in 2050 in their “high scenario” and a low air-traffic growth and optimistic technology development reaching 2.17 TgN yr⁻¹ in 2050 for the “low scenario”, intermediate between the A1B and B1 scenarios in terms of NO_x emissions. The ACCRI 2050-S1 scenario also provides emissions intermediate between the A1B and B1 scenarios in terms of global NO_x and BC emissions. The SSP3-7.0 scenario, used as a reference in the AerChemMIP model intercomparison (Collins et al., 2017), also provides NO_x emissions intermediate between the QUANTIFY_A1 and QUANTIFY_B1 and BC and SO₂ emissions close to QUANTIFY_A1. The mitigation scenario SSP1-2.6, also used as a mitigation option for the AerChemMIP simulations, is close to the QUANTIFY_B1_ACARE in terms of global emissions. This comparison suggests that the benchmark QUANTIFY scenarios used in this study are generally consistent with more recent aircraft scenarios in terms of global mean emissions and provide a reasonable estimate for both baseline and mitigation scenarios.

300

3 The LMDZ-INCA model

3.1 Model description

305 The LMDZ-INCA global chemistry-aerosol-climate model couples on-line the LMDZ (Laboratoire de
Météorologie Dynamique, version 6) General Circulation Model (Hourdin et al., 2020) and the INCA (INteraction
with Chemistry and Aerosols, version 5) model (Hauglustaine et al., 2004; 2014). The interaction between the
atmosphere and the land surface is ensured through the coupling of LMDZ with the ORCHIDEE (ORganizing
Carbon and Hydrology In Dynamic Ecosystems, version 1.9) dynamical vegetation model (Krinner et al., 2005).
310 In the present configuration, we use the “Standard Physics” parameterization of the GCM (Boucher et al., 2020).
The model includes 39 hybrid vertical levels extending up to 70 km. The horizontal resolution is 1.9° in latitude
and 3.75° in longitude. The primitive equations in the GCM are solved with a 3 min time-step, large-scale transport
of tracers is carried out every 15 min, and physical and chemical processes are calculated at a 30 min time interval.
For a more detailed description and an extended evaluation of the GCM we refer to Hourdin et al. (2020). The
315 large-scale advection of tracers is calculated based on a monotonic finite-volume second-order scheme (Van Leer,
1977; Hourdin and Armengaud 1999). Deep convection is parameterized according to the scheme of Emanuel
(1991). The turbulent mixing in the planetary boundary layer is based on a local second-order closure formalism.
The transport and mixing of tracers in the LMDZ GCM have been investigated and evaluated against observations
for both inert tracers and radioactive tracers (e.g., Hourdin and Issartel, 2000; Hauglustaine et al., 2004) and in the
320 framework of inverse modelling studies (e.g., Bousquet et al., 2010; Zhao et al., 2019).

INCA initially included a state-of-the-art CH₄-NO_x-CO-NMHC-O₃ tropospheric photochemistry (Hauglustaine et
al., 2004; Folberth et al., 2006). The tropospheric photochemistry and aerosols scheme used in this model version
is described through a total of 123 tracers including 22 tracers to represent aerosols. The model includes 234
325 homogeneous chemical reactions, 43 photolytic reactions and 30 heterogeneous reactions. Please refer to
Hauglustaine et al. (2004) and Folberth et al. (2006) for the list of reactions included in the tropospheric chemistry
scheme. The gas-phase version of the model has been extensively compared to observations in the lower
troposphere and in the upper troposphere. For aerosols, the INCA model simulates the distribution of aerosols with
anthropogenic sources such as sulfates, nitrates, black carbon (BC), organic carbon (OC), as well as natural
330 aerosols such as sea salt and dust. The heterogeneous reactions on both natural and anthropogenic tropospheric
aerosols are included in the model (Bauer et al., 2004; Hauglustaine et al., 2004; 2014). The aerosol model keeps
track of both the number and the mass of aerosols using a modal approach to treat the size distribution, which is
described by a superposition of 5 log-normal modes (Schulz, 2007), each with a fixed spread. To treat the optically
relevant aerosol size diversity, particle modes exist for three ranges: sub-micronic (diameter < 1 μm) corresponding
335 to the accumulation mode, micronic (diameter between 1 and 10 μm) corresponding to coarse particles, and super-
micronic or super coarse particles (diameter > 10 μm). This treatment in modes is computationally much more
efficient compared to a bin-scheme (Schulz et al., 1998). Furthermore, to account for the diversity in chemical
composition, hygroscopicity, and mixing state, we distinguish between soluble and insoluble modes. In both sub-
micron and micron size, soluble and insoluble aerosols are treated separately. Sea-salt, SO₄, NO₃, and methane
340 sulfonic acid (MSA) are treated as soluble components of the aerosol, dust is treated as insoluble, whereas black
carbon (BC) and organic carbon (OC) appear both in the soluble and insoluble fractions. The ageing of primary
insoluble carbonaceous particles transfers insoluble aerosol number and mass to soluble with a half-life of 1.1 day.
Ammonia and nitrates aerosols are considered as described by Hauglustaine et al. (2014). The aerosol component
of the LMDZ-INCA model has been extensively evaluated during the various phases of AEROCOM (e.g., Glibb et
345 al., 2021; Bian et al., 2017).

Earlier versions of the LMDZ-INCA model only including gas-phase tropospheric chemistry have been previously
used to assess the impact of subsonic aircraft on tropospheric ozone (Koffi et al., 2010; Hauglustaine and Koffi,
2012). These previous versions of the LMDZ-INCA model were prescribing the ozone distribution to satellite
350 observations above a potential temperature of 380K, providing a strong constraint on the ozone perturbation at
aircraft flight altitudes. In order to assess the impact of aircraft emissions on atmospheric composition, the model
has been extended to include an interactive chemistry in the stratosphere and mesosphere. Chemical species and
reactions specific to the middle atmosphere have been included. A total of 31 species were added to the standard
chemical scheme, mostly belonging to the chlorine and bromine chemistry, and 66 gas phase reactions and 26
355 photolytic reactions. Water vapour is now affected by both physical processes in LMDZ and, in the stratosphere,
an additional H₂O tracer is introduced in INCA in order to account for photochemical production and destruction.
In addition, heterogeneous processes on Polar Stratospheric Clouds (PSCs) and stratospheric aerosols are
parameterized in INCA following the scheme implemented in Lefèvre et al. (1994). PSCs are first predicted as a
function of H₂O and HNO₃ local partial pressures, using the saturation vapour pressures for type I PSC (nitric acid
360 trihydrate crystals) and for type II water-ice PSC (Hanson et al. 1988, Carslaw et al. 1995). The excess of H₂O and
HNO₃ is removed from the gas phase when saturation occurs and is used to compute the surface area concentration
in the PSC region. Heterogeneous reaction rates are calculated explicitly, as a function of the surface area available,
mean molecular velocity, and the reaction probabilities. Furthermore, the PSC scheme includes sedimentation of
the cloud material. The fallout of PSC particles affects the vertical distribution of H₂O, HNO₃, and HCl. Condensed
365 species are returned to the gas phase when clouds evaporate. In the presence of PSCs, the heterogeneous reactions
convert bromine and chlorine reservoirs (HCl, HBr, ClONO₂, BrONO₂) into reactive species (Cl₂, ClNO₂, HOCl,

Br₂, BrNO₂, HOBr) based on 9 additional heterogeneous reactions introduced in the chemical scheme. The distribution of stratospheric aerosols is prescribed according to the CCMI exercise (Thomason et al., 2018).

370 3.2 Model evaluation

We mostly refer to previous publications for a general evaluation of the LMDZ-INCA model performances and comparison against observations for both gas phase chemistry and aerosols (e.g., Brunner et al., 2003, 2005; Hauglustaine et al., 2004; Folberth et al., 2006; Myhre et al., 2013; Hauglustaine et al., 2014; Koffi et al. 2016).
375 The version of the LMDZ-INCA model used in this study and extended to the stratosphere has been evaluated by comparing model outputs with observations, in particular in the upper-troposphere and lower-stratosphere, before the model has been applied to investigate the impact of aircraft emissions. In this study, we summarize this evaluation for two key observational datasets.

380 **Figure 1** summarizes the assessment of the modelled ozone seasonal cycle against ozonesondes as compiled by Tilmes et al. (2012) and with respect to the latitude and pressure domains. We present Taylor diagrams to summarize the model biases and correlations with the dataset. The model results are interpolated on both the horizontal and 16 pressure levels to mimic the 42 ozonesonde stations observations over the 1995-2011
385 observational period. The pressure levels are further grouped into pressure ranges represented by a different color for a sake of clarity. In terms of yearly mean biases, we distinguish two distribution modes for the three geographical domains, although it is less visible in the tropics (0-30°): the 100 – 200 hPa pressure range (corresponding to the lower stratosphere in the middle (30-60°) and high (60-90°) latitudes), and the other pressure intervals throughout the troposphere. On one hand, the 200 – 1000 hPa mean values show a tendency towards negative biases, especially at high-latitudes where the modelled yearly averages spread from about 60% to 100%
390 with respect to the observations, contrasting with the 80 to 110 % interval elsewhere. On the other hand, most of 100 – 200 hPa yearly mean values are positively biased. In the middle and high latitudes, almost all the significant positive biases concern this pressure domain.

In matter of correlation between observed and modelled seasonal cycles, Pearson's r coefficient mainly spreads
395 from 0.60 up to 0.95, and is mostly greater than 0.8. Outside the tropics, this metric also shows distinct distribution modes between the same pressure domains. Higher correlations are reported in the 100 – 200 hPa interval where most r values are greater than 0.9 and part of them even reach the 0.99 value. Note that the six high-latitude points showing a poor correlation and a strong positive bias correspond to the three stations located in the southern polar region (Marambio, 64°S; Syowa, 69°S; Neumayer, 70°S) at 125 and 150 hPa. Consequently, although the
400 simulation tends to overestimate lower-stratospheric ozone in the middle and high latitudes, it reproduces the seasonality particularly well outside the southern pole.

Figure 2 provides, again as Taylor diagrams, the assessment of the modelled geographical distribution against
405 IAGOS observations for ozone and CO, averaged over the periods December 1994 – November 2017 and December 2001 – November 2017 respectively (Cohen et al., 2018). The IAGOS (In-service Aircraft for a Global Observing System, www.iagos.org) is a European research infrastructure performing *in situ* measurements on board several passenger aircraft (Petzold et al., 2015). Amongst the observed variables, ozone and CO have been monitored so far since August 1994 and December 2001, respectively. Information on the instruments is available in Thouret et al. (1998) and Marenco et al. (1998) for ozone and in Nédélec et al. (2003, 2015) for CO. The model
410 assessment against the aircraft-based measurements is performed using the Interpol-IAGOS software (Cohen et al., 2021) that consists in projecting the IAGOS data onto the model grid and to derive monthly means for each sampled grid cell. The model monthly averages are then derived from the daily output by applying a mask with respect to the IAGOS sampling. Last, for each data set, these monthly outputs are used to derive seasonal and annual climatologies. For this comparison we apply the methodology for comparison with the global model
415 described in Cohen et al. (2021). Since all the four cruise-altitude levels are regularly crossed by the tropopause, each of them will contain both high-ozone (low-CO) and low-ozone (high-CO) grid cells. In order to account for these discrepancies while deriving a mean bias, thus to avoid absolute biases in high values to govern the results, the normalized mean value shown in these graphics is derived from the Modified Normalized Mean Bias (MNMB).

420 In yearly means, the normalized mean value for ozone spreads from about 70% up to 125% and increases with the altitude, consistently with **Fig. 1**. It is also the case with the dependence on the season, represented by a 10% difference at 300 hPa and a 30% difference at 180 hPa. The same scheme is reproduced between the three highest levels, i.e. a lower summertime value and a greater wintertime value, likely depending on the distance from the tropopause. It suggests that the vertical ozone gradient in the lower stratosphere is overestimated by the model.
425 However, the ozone geographical distribution is remarkably well correlated between the simulation and the observations, with all the yearly r coefficients greater than 0.92. It is especially the case at the highest levels. One possible reason is a good representation of tropopause motions at northern mid-latitudes, which ensures a realistic proportion between stratospheric and tropospheric air masses in most grid cells. Carbon monoxide is characterized by relatively small biases at the IAGOS-coverage scale, showing a balance between regional positive and negative
430 biases. As for ozone, the correlation increases with altitude. However, the poor correlation reported at the lowest level highlights the difficulties to simulate the upward transport of pollutants in the troposphere.

435 The distribution of aerosol surface concentrations (sulfates, nitrates, ammonium) calculated with this version of
the model has been evaluated and compared to surface stations by Hauglustaine et al. (2014) over Europe and
Northern America and by Li et al. (2016) over China and is not repeated here. However, **Fig. S2** compares the
calculated total Aerosol Optical Depth (AOD) at 550 nm to the AERONET and MODIS observations for Eastern
and Central China, Western Europe and the Eastern United-States. A very good agreement is obtained with
MODIS data with biases of -10%, 1.4% and -6.1 % for these three regions, respectively, and a correlation
440 coefficient r of 0.59, 0.55 and 0.86. Larger biases are calculated against AERONET data, in particular over regions
characterized with very high aerosol loading such as China. Biases of respectively -39%, 10% and 24% are
obtained for the three regions with correlation coefficients of 0.5, 0.45, and 0.78.

3.3 Model set-up

445 In this study, meteorological data from the European Centre for Medium-Range Weather Forecasts (ECMWF)
ERA-Interim reanalysis have been used. The relaxation of the GCM winds towards ECMWF meteorology is
performed by applying at each time step a correction term to the GCM u and v wind components with a relaxation
time of 2.5 hours (Hourdin and Issartel, 2000; Hauglustaine et al., 2004). The ECMWF fields are provided every
6 hours and interpolated onto the LMDZ grid. We focus this work on the impact of aircraft emissions on
450 atmospheric composition, its future evolution, and its direct radiative forcing of climate. In order to isolate the
impact of aircraft emissions, all snapshot simulations are performed under present-day climate conditions and run
for a period of ten years after a two-year spin-up. Therefore, ECMWF meteorological data for 2000–2009 are used.
The perturbations are averaged over the last 3 years of the simulations. The impact of future climate change on
aircraft perturbations is however an interesting topic to be investigated in forthcoming studies.

455 For the baseline simulations, the anthropogenic emissions compiled by Lamarque et al. (2010), are added to the
natural fluxes used in the INCA model. The ORCHIDEE vegetation model has been used to calculate off-line the
biogenic surface fluxes of isoprene, terpenes, acetone and methanol as well as NO soil emissions as described by
Lathi re et al. (2005). NH₃ emissions from natural soils and ocean are taken from Bouwman et al. (1997). Natural
460 emissions of dust and sea salt are computed using the 10m wind components from the ECMWF reanalysis. For
the future simulations (2050), the Representative Concentration Pathways (RCP) 6.0 anthropogenic and biomass
burning emissions provided by Lamarque et al. (2011) are used. Natural emissions for both gaseous species and
particles are kept to their present-day level. Lightning is an important source of NO_x in the upper-troposphere at
aircraft cruise altitudes. The lightning NO_x emissions are parameterized in the model based on convective cloud
465 heights as described in Jourdain et al. (2001). Based on this parameterization, the total lightning NO_x emissions
for the baseline simulation is 5.5 TgN/yr. The methane surface mixing ratio used for both chemistry simulations
and radiative forcing calculations is fixed to 1769 and 1895 ppbv for the “present-day” (2006) and 2050 baseline
simulations, respectively. For N₂O, the surface mixing ratio is fixed to 323 and 355 ppbv for 2006 and 2050,
respectively.

470 The impact of aviation emissions on atmospheric composition is calculated based on a 100% perturbation
methodology, comparing the results of the simulations with aircraft emissions to a reference simulation with zero
aircraft emissions. As discussed by S vde et al. (2014), in previous work, both 5% perturbations (e.g. Hoor et al.,
2009; Hodnebrog et al., 2012) and 100% perturbations (e.g., Gauss et al., 2006, S vde et al., 2014) have been
475 applied. Koffi et al. (2010) compared the two methodologies and found that the 100% perturbation of transport
emissions induces a 6% higher transport-induced ozone burden perturbation in the case of aircraft emissions. As
noted by S vde et al. (2014) the small perturbation approach is more adapted when different transport modes,
affected differently by non-linearities, are compared. The 100% perturbation gives the overall effect of aircraft,
without considering compensating effects from other emission sectors due to chemical non-linearity (Koffi et al.,
480 2010; S vde et al. 2014; Grewe et al., 2019). This non-linear chemistry depends mostly on the background of NO_x
and hydrocarbons, and increases with larger perturbations in NO_x. In this study we focus on aircraft emissions
solely in contrast to other studies which compared impact of emissions from different transport modes (e.g., Hoor
et al., 2009; Koffi et al., 2010; Hodnebrog et al., 2012). Sensitivity analysis (as we envisaged our simulations)
aims at characterizing the concentration change resulting from a given emissions change (Clappier et al., 2017).
485 On the other hand, source apportionment approaches aim to quantify contributions by attributing a fraction of the
pollutant concentration to each emission source (e.g., tagged species approach) (Grewe et al., 2010; Clappier et
al., 2017; Grewe et al., 2019; Matthes et al., 2021). The two methods provide different results but also different
information. The source apportionment accounts for non-linearities and is used to retrieve information on the
source contribution to the concentration of one pollutant (e.g., contributions of different transport modes to ozone).
490 Sensitivity or impact methods are used to determine the impact of abatement strategies. In this study which focuses
on aircraft impact solely, we adopt the 100% perturbation, keeping in mind this may mask some mild non-
linearities. **Table 3** summarizes the simulations performed and analyzed in this study.

3.4 Radiative forcing calculations

495 Several radiative forcings associated with atmospheric composition changes due to aircraft emissions are
computed on-line during the LMDZ-INCA simulations. This is in particular the case for the various components
of the direct aerosol forcing. The radiative calculations in the GCM are based on an improved version of the

500 ECMWF scheme developed by Fouquart and Bonnel [1980] in the solar part of the spectrum and by Morcrette [1991] in the thermal infrared. The shortwave spectrum is divided into two intervals: 0.25–0.68 μm and 0.68–4.00 μm . The model accounts for the diurnal cycle of solar radiation and allows fractional cloudiness to form in a grid box. These radiative forcings are calculated as instantaneous, clear-sky and all-sky forcings at the surface and at the top of the atmosphere. In section 6 the all-sky forcings at the top of the atmosphere will be presented for aerosols as was done for instance by Hauglustaine et al. (2014).

505 For ozone and stratospheric water vapour, a different protocol is used. For these two species, the radiative forcings at the tropopause are calculated with an off-line version of the LMDZ GCM radiative transfer model described above. In this off-line version, the forcings are calculated on a monthly mean basis using the temperature, water vapour, cloud distributions and optical properties, surface albedo, and ozone fields stored from the GCM
510 simulations and read from pre-established history files. The fixed-dynamical heating approximation is then applied to the calculations with a thermal adjustment of the stratosphere. The radiative code iterates until the forcings at the top of the atmosphere converges with the forcings at the tropopause. The iterations are performed with a one-day timestep over 200 days. This radiative transfer model off-line of the LMDZ-INCA model has for instance
515 already been used to calculate the tropospheric ozone radiative forcings in Berntsen et al. (2005) or more recently in Li et al. (2016).

As described in previous work (e.g., Fuglestedt et al., 1999; Skowron et al., 2013), the decrease in methane
520 mixing ratio due to aircraft NO_x emissions and associated with enhanced oxidation by OH, is responsible for a long-term methane direct radiative forcing that we calculate at equilibrium based on the change in the methane photochemical lifetime, and including the methane feedback on its own lifetime. According to this methodology the steady-state methane mixing ratio decrease due to aircraft emissions is given by (Prather, 1994; Fiore et al., 2009; Holmes, 2018):

$$525 \quad q_{\text{CH}_4} = q_{\text{CH}_4}^0 (1 + f \Delta\tau_{\text{CH}_4}) \quad (1)$$

where q_{CH_4} is the new steady-state methane mixing ratio, $q_{\text{CH}_4}^0$ is the reference methane mixing ratio (taken as 1769 ppbv for the “present-day” and 1985 ppbv in 2050), f denotes the methane feedback on its own lifetime (Prather et al., 2001; Holmes et al., 2011), and $\Delta\tau_{\text{CH}_4}$ (%) is the change in the methane lifetime due to aircraft
530 emissions and subsequent OH perturbation. The associated direct radiative forcing of climate of this change in methane is calculated using the simple formula revised by Etminan et al. (2016). As reported by these authors, the inclusion of the shortwave contribution in this revised expression results, for instance, in an increase by 24.5% of the methane forcing associated with a halving of its concentration, compared to the previous literature (Myhre et al., 1998). For the methane feedback factor, f , Prather et al. (2001) derived a best estimate value of 1.4 based on a multimodel range of 1.33–1.45. A similar best estimate value was recommended by Holmes et al. (2011). Fiore et al. (2009) derived a multimodel ensemble mean of 1.33 and a range of 1.25–1.43, including a value of 1.31
535 contributed with an earlier version of the LMDZ-INCA model. The feedback factor has been recalculated in this study for the current version of our model based on a reference simulation and a 10% perturbation in methane surface mixing ratio simulation. Based on this set of simulations and the methodology described in Fiore et al. (2009), we recalculated a methane feedback factor f of 1.36, in agreement with the previous estimates. This factor
540 is then used in Eq. (1) in order to derive the change in methane mixing ratio due to aircraft emissions and the associated radiative forcing of climate. It should be noted that this estimate of the methane feedback is based on fixed surface CH_4 concentrations. Other methodologies have also been proposed to evaluate this feedback and in particular the use of methane surface fluxes (Khodayari et al., 2015; Pitari et al., 2016). Khodayari et al. (2015) concluded that for the simulations with fixed CH_4 at the lower boundary condition, the parameterization based on
545 Eq. (1) using the global mean lifetime approach overestimates the change in CH_4 by 8.6% compared to the change calculated directly from the model using CH_4 surface emissions. The overestimation is 12.1%–20.0% if using other lifetime approaches. They concluded that the parameterization based on Eq. (1) is good to within $\sim 10\%$ when using the global mean lifetime approach.

550 The indirect forcings associated with this change in methane mixing ratio through long-term tropospheric ozone and stratospheric water-vapour adjustments were recalculated with the LMDZ-INCA global model. This was done by imposing the new methane steady-state surface mixing ratio q_{CH_4} (1744 ppbv) calculated from Eq. (1) for the “present-day” REACT4C_2006 simulation in the 3D model and running for a period of 10 years in order to determine the associated change in ozone and stratospheric water vapour by comparing to a reference simulation
555 using $q_{\text{CH}_4}^0$ (1769 ppbv) as methane surface mixing ratio. In this case, we calculated a change in ozone after 10 years of -0.93 Tg (0.085 DU) and a change in stratospheric water vapour of -2.12 Tg . We then calculated for these perturbations, an ozone and a stratospheric water vapour radiative forcings. These calculations provide an indirect long-term ozone forcing of $116 \text{ mW/m}^2/\text{ppmv}$ of CH_4 and an indirect long-term stratospheric water vapour forcing of $27 \text{ mW/m}^2/\text{ppmv}$ of CH_4 . The ozone forcing is smaller by 17% compared to the value of $140 \pm 70 \text{ mW/m}^2/\text{ppmv}$ provided by Forster et al. (2021) but well within the provided confidence level. For stratospheric H_2O , the forcing
560 is subject to a larger uncertainty, and we derive a forcing lower by 32% compared to the value of $40 \pm 40 \text{ mW/m}^2/\text{ppmv}$ provided by Forster et al. (2021) but also well within the confidence level. These calculated forcings were then used to derive the indirect long-term ozone and water vapour forcings for the other aircraft emission

565 scenarios based on a simple scaling with the methane mixing ratio change calculated with Eq. (1) for all simulations.

Carbon dioxide is the end-product of the methane atmospheric oxidation. The production of CO₂ is hence an indirect radiative forcing resulting from the change in methane mixing ratio due to increased oxidation by OH resulting from aviation NO_x emissions. Since intermediate carbon containing methane oxidation products are
570 subject to dry and wet deposition, not every oxidized methane molecule results in a produced CO₂ molecule. In this study, we assume that 1 mole of change in CH₄ oxidation leads to 0.6 mole of CO₂ produced (Folberth et al., 2005; Boucher et al., 2009). The decrease in CH₄ due to enhanced oxidation is then translated into a change in CO₂ and converted to a radiative forcing based on the simple formula from Myhre et al. (1998). Based on the REACT4C_2006 change in methane mixing ratio we derive an indirect CO₂ forcing $F_{CH_4-CO_2}$ of 8.25 mW/m²/ppmv
575 of CH₄. This normalized number is used to calculate the forcings for the other simulations.

4 “Present-day” baseline perturbations

4.1 Aviation impact on atmospheric composition

580 **Figure 3** presents the daily changes in concentration associated with the base REACT4C_2006 aircraft emission inventory for several key species at 250 hPa (i.e. cruise altitude). For NO_x, a strong seasonal cycle is calculated with a fall-winter maximum reaching 39 pptv and a summer minimum of 15-20 pptv located at 30°-60°N and corresponding mostly to the transatlantic flight corridors. A northward transport of NO_x, associated with the
585 transport of mid-latitude air masses to the polar regions is visible. During spring, the NO_x mixing ratio increases by up to 20 pptv at high latitudes. The geographical distribution depicted in **Fig. 4** shows that NO_x increases by up to 60 pptv in regions with high aircraft emissions over Europe, Northern America. It also extends to North-East Asia and Japan, reaching more than 40 pptv. As a consequence of this increase in NO_x concentrations, ozone increases by 3-6 ppbv at flight altitude at northern mid-latitudes. A marked seasonal cycle (**Fig. 3**), associated with
590 the NO_x increase and higher photochemical activity, is calculated at mid-high northern latitudes and peaks in May. This maximum reached in May at high latitudes is the result of a combination of a more intense photochemical activity in summer combined with a more intense transport poleward in spring. As a consequence, the peak is reached at the end of the spring season. A maximum zonal mean ozone increase reaching almost 7 ppbv is calculated in polar regions where photochemistry is active and where mid-latitude ozone is transported and
595 accumulates. Due to its longer lifetime, the change in ozone at 250 hPa reaches 2-4 ppbv over most of the northern hemisphere above 30°N (**Fig. 4**).

The zonal mean distributions of the NO_x and O₃ perturbations are shown in **Fig. 5** for January and May. These two months are chosen in order to illustrate the minimum and maximum perturbations in atmospheric composition.
600 The NO_x increase reaches a maximum of about 45 pptv (60%) at 250 hPa and at 40°N-60°N during both seasons. In May, the mixing of air masses towards higher latitudes is visible with increased mixing ratios reaching about 25 pptv at the pole. The induced ozone perturbation ranges from a maximum of 3 ppbv in January to a maximum of 6-7 ppbv in May (4%). These results agree with the model intercomparison of Søvdé et al. (2014) who calculated, with the same aircraft emission inventory, a maximum ozone increase ranging from 4.8 to 8.8 ppbv
605 during summer, and a lower impact in winter associated with less photochemical activity, and ranging from 3.4 to 4.4 ppbv. They are also in agreement in terms of distribution and ozone increase with the earlier model intercomparison results by Hoor et al. (2009) obtained with the QUANTIFY_2000 emission inventory, and with the peak absolute ozone increase of 5 to 8 ppbv calculated by Olsen et al. (2013). The calculated maximum ozone perturbation occurs between 300 and 200 hPa in both seasons. A downward transport of the ozone produced is visible down to 800 hPa at 30°N-40°N. Due to higher photochemical activity at high latitudes (>60°N), and mixing
610 and accumulation of air masses around the pole, the ozone increase is centered in polar regions in May. In winter, this maximum is located at lower latitudes between 40°N and 60°N, as illustrated in **Fig. 4**. The maximum perturbation associated with aircraft emissions appears just above the tropopause at high latitudes showing the need to account for both chemistry in the troposphere and in the stratosphere (Gauss et al., 2006; Søvdé et al., 2014; Khodayari et al., 2014a). As a result of the NO_x and hence ozone increases, an increase of OH located
615 between 30°N and 50°N, depending on the solar radiation seasonal cycle, and reaching 14-20 10⁻³ pptv is calculated (**Fig. 3**).

The increase in water vapour associated with H₂O aircraft emissions shows a strong seasonal cycle and reaches a
620 maximum of 3.5 ppbv in spring at 250 hPa (**Fig. 3**). The zonal mean distribution (**Fig. 5**) shows that the maximum is located in the stratosphere where the water vapour lifetime is longer. The increase in stratospheric water vapour reaches 19 ppbv (0.2%) at 200 hPa in January at 60°N. In May the increase reaches about 10 ppbv at this latitude. This is significantly lower than the 64 ppbv annual mean maximum increase calculated by Wilcox et al. (2012) with a Lagrangian model and considering water vapour as a passive tracer. With a Lagrangian model, Morris et al. (2003) also calculated an increase of water vapour due to aircraft emissions of more than 150 ppbv just above
625 the tropopause and of less than 2 ppbv in the stratosphere. In our model set-up, the increase of water vapour is reset to zero below the model tropopause at each time-step, strictly limiting the aircraft perturbation to a stratospheric perturbation.

630 For BC (**Fig. 3**), the seasonal cycle is well marked with a maximum reaching 0.16 ng/m^3 in winter-spring and a
minimum in summer of 0.01 ng/m^3 . This aerosol accumulates at cruise altitude during winter leading to a marked
635 maximum. In summer, due to more intense atmospheric mixing, these high concentrations are mixed to lower
altitudes. Meridional and poleward transport is also visible for these particles and higher concentrations are
reached from 40°N to the pole, in agreement with the transport of NO_x discussed earlier. The change in SO_2
concentration (not shown) exhibits a similar feature with a winter maximum reaching more than 6 pptv. For this
aerosol precursor, despite direct aircraft emissions, a decrease is calculated in summer reaching 3.5 pptv, and
640 corresponding to the SO_2 oxidation by OH forming sulfate particles. As a consequence of this enhanced
production, a maximum increase in SO_4 is calculated from May to September and reaches $8\text{-}12 \text{ ng/m}^3$ (**Fig. 3**).

640 **Figure 6** shows the geographical distribution of the BC perturbation at 250 hPa. In January, the maximum reaching
 0.17 ng/m^3 is located over source regions in Northern America, Europe and Eastern Asia with zonal transport over
the Pacific and Atlantic flight corridors. The distribution in May clearly shows transport and accumulation of BC
in polar regions. The zonal mean distribution of the BC perturbation is shown in **Fig. 7** and exhibits a maximum
645 of 0.15 ng/m^3 (1%) between 300 and 200 hPa at 40°N - 70°N . A redistribution of these flight altitude emissions
through subsidence is visible with a secondary maximum of about 0.08 ng/m^3 (0.15%) calculated in the lower
troposphere around 30°N . These results are in line with the perturbations calculated by Righi et al. (2016) and
ranging from $0.05\text{-}0.1 \text{ ng/m}^3$ in annual mean at cruise altitude in the northern hemisphere. In the lower troposphere,
Righi et al. (2016) calculated a somewhat higher BC concentration increase reaching up to 0.5 ng/m^3 near the
650 surface.

The geographical distribution of sulfates at 250 hPa (**Fig. 6**), clearly shows a strong seasonal cycle associated with
increased oxidation of SO_2 in spring, reaching $14 \mu\text{g/m}^3$ in May over a large part of Europe and Asia. In **Fig. 7**,
the zonal mean SO_2 perturbation varies between 8 ppt (40%) in January and 5 ppt (30%) in May at 200 hPa
655 between 40°N and 90°N . The associated sulfate perturbation reaches a maximum of 10 ng/m^3 (4%) in May with a
minimum of 5 ng/m^3 (3%) simulated in January and localized, as for BC, between 300 and 200 hPa at the latitude
band between 30°N - 50°N and with a clear poleward transport in May. As seen for BC, a significant subsidence of
the sulfate perturbation is calculated between 30 and 40°N . Again, these results agree with the perturbations
calculated by Righi et al. (2016) with the EMAC model and reaching $2\text{-}5 \text{ ng/m}^3$ in annual mean at cruise altitude
660 in the northern hemisphere. In the lower troposphere, Righi et al. (2016) calculated higher SO_4 concentration
increase reaching up to 10 ng/m^3 near the surface. Since similar emission indexes are used in both studies, this
points towards a more efficient removal of aerosols in LMDZ-INCA than in EMAC.

Nitrates are not emitted by aviation but their distribution is affected by two competing processes. On one hand,
665 the increase of SO_4 reduces the amount of NH_3 available for ammonium nitrate formation and on the other hand
the increase of NO_x enhances the production of nitrates. At cruise altitudes, the strong increase in SO_4 dominates
and an overall decrease in nitrates of up to $-7 \mu\text{g/m}^3$ (7%) is calculated in May over Europe and Asia, collocated
with the increase in sulfates (**Fig. 6**). In regions characterized with high NH_3 concentrations, in India or south-east
Asia, enough ammonia is still present after ammonium sulfate production to increase the production ammonium
670 nitrate when more NO_x associated with aircraft emissions are present. This is in particular the case in January
around 30°N in the lower troposphere (**Fig. 7**), but also at cruise altitudes in localized areas in India and South-
East Asia (**Fig. 6**). In these regions an increase of nitrates reaching more than 9 ng/m^3 is calculated. Righi et al.
(2016) calculated a very similar zonal mean pattern for the nitrate concentration perturbation, decreasing in the
upper troposphere by up to $1 \mu\text{g/m}^3$ in annual mean and increasing by $5\text{-}10 \text{ ng/m}^3$ in the lower troposphere.
675 Similarly, the zonal mean perturbation pattern for nitrate aerosols agrees with the results presented by Unger
(2011).

4.2 Impact of flight altitude changes

680 The atmospheric lifetime of pollutants emitted by aviation is highly dependent on the altitude at which they are
injected into the atmosphere (Grewe et al., 2002; Gauss et al., 2006; Fröming et al., 2012; Søvde et al., 2014;
Matthes et al., 2017). The sensitivity of the calculated perturbations to the flight altitude is illustrated in this section
based on the REACT4C_PLUS and REACT4C_MINUS emissions corresponding, respectively, to an increase or
decrease of the flight cruise altitude by 2000 feet compared to the REACT4C_2006 baseline inventory.

685 **Figure 8** shows the impact of the flight altitude variation on the zonal mean distribution of key species compared
to the baseline scenario. These variations are illustrated for May conditions when the maximum impact of aircraft
emissions is calculated by the model, as illustrated in the previous section. As expected as a consequence of the
chemical lifetime increase with altitude, a higher (resp. lower) flight cruise altitude increases (resp. decreases) the
690 change in ozone mixing ratio by 1.7 ppbv (30%) (resp. -1.6 ppbv) between 150 and 250 hPa compared to the
baseline scenario. The impact on ozone is comparable to the results obtained by Søvde et al. (2014) and Matthes
et al. (2017; 2021) (1-2 ppb in summer and 0.4-1 ppb in winter). Similarly, the BC concentration increases by
 0.031 ng/m^3 (20%) when the flight altitude is increased and, in contrast, decreases by 0.032 ng/m^3 with a lowered
flight altitude.

695 Directly related to the response of SO₂ to flight altitude changes, the concentration of sulfates shows a behavior similar to the primary aerosol BC, and increases by a maximum of 2.3 ng/m³ (22%) between 250 and 150 hPa at 40°-90°N in the REACT4C_PLUS case and decreases by 2.3 ng/m³ in the REACT4C_MINUS simulation. In contrast, the variation of nitrate aerosols shows an opposite behavior associated to the change in sulfates. An increase in sulfates reduces the NH₃ available for forming ammonium nitrates particles in favor of ammonium sulfates and NO₃ decreases by 0.84 ng/m³ (23%) at flight altitude in the REACT4C_PLUS simulation. Please note that the change in sulfates is maximum at high latitudes but the maximum perturbation in nitrates occurs at lower latitudes (around 30°N) where more NH₃ is present at this altitude. Similarly, the decrease in sulfate concentration calculated in the REACT4C_MINUS scenario induces an increase of ammonium nitrate particles of 0.83 ng/m³ at 200 hPa. These sensitivity simulations show that changing the aircraft flight altitude has a marked impact on the ozone and aerosol responses to emissions (of about 20-30% compared to the baseline simulation in May) and hence on the associated radiative forcings, as will be analyzed in the section 6.

5 Future impact of aviation

710 5.1 Future baseline scenario

In addition to these simulations using the REACT4C_2006 emission inventory, a set of future simulations using the QUANTIFY emission inventories has been carried out for the year 2050. The corresponding distributions of the baseline perturbations for the QUANTIFY_2000 inventory are in line with the results obtained for REACT4C_2006 (**Fig. S3**). However, in the case of the QUANTIFY_2000 emissions, due in particular to the higher fuel consumption, the maximum perturbations are generally slightly higher. In zonal mean, these perturbations reach 6.8 ppbv for ozone in May between 250 hPa and 350 hPa, 0.16 ng/m³ for BC, 11.3 ng/m³ for SO₄, and -3.95 ng/m³ for NO₃, to be compared with 6.4 ppbv, 0.15 ng/m³, 10.2 ng/m³ and -3.71 ng/m³, respectively, in the case of REACT4C_2006 (see Section 4).

720 For future simulations (2050), the baseline simulation corresponds to the aviation emissions from the QUANTIFY_A1 inventory. **Figure 9** illustrates the perturbation associated with aircraft emissions for this scenario for key constituents (May as the seasonal maximum of the perturbation). The NO_x mixing ratio increases in the upper troposphere by up to 194 pptv in January at 200 hPa and 170 pptv (250%) in May (not shown). As a consequence, ozone increases from 9.2 ppbv in January to up to 19.6 ppbv (15%) in May at flight altitude. These values are comparable to the values calculated by Søvde et al. (2007) (7 to 18 ppbv for monthly averages in January and May respectively) but higher than the ozone increase calculated by Koffi et al (2010) (10 ppbv in July) and the model mean given by Hodnebrog et al. (2012) for the same emission inventory. We note however that only a few models used in Hodnebrog et al. (2012) included an interactive chemistry in the stratosphere, hence imposing ozone to climatologies or calculated with simplified parameterizations in this region. This could have the consequence to dampen the response of ozone in the upper-troposphere. This finding is confirmed by the higher tropospheric ozone increase associated with aircraft NO_x emissions calculated by global models including both interactive chemistry in the troposphere and in the stratosphere (Olsen et al., 2013; Khodayari et al., 2014a; Brasseur et al., 2016; Skowron et al., 2021). The increase in BC is also significant and reaches 0.6 ng/m³ in January and 0.55 ng/m³ (5%) in May, a factor of 3 larger than the QUANTIFY_2000 perturbation. As noted earlier, in addition to the maximum increase at flight altitude, a secondary maximum reaching 0.3 ng/m³ and associated with the downward redistribution of aircraft emissions is also calculated at ground level. The increase in SO₄ for this scenario reaches 15.6 ng/m³ in January and 32.8 ng/m³ (15%) in May. The marked increase in SO₄ concentrations at cruise altitude is responsible for a subsequent decrease in NO₃ reaching -9.4 ng/m³ and -21 ng/m³ in May (50%). Below about 500 hPa, an increase in NO₃ concentrations reaching 14 ng/m³ (10%) in May and as much as 47 ng/m³ (5%) in January is simulated. These increased surface concentrations in 2050 are mostly associated with much higher NH₃ background concentrations at the surface in the future (in particular in South East Asia) (Hauglustaine et al., 2014), and subsequent enhanced NO₃ formation due to redistribution of aircraft NO_x emissions to lower levels forming ammonium nitrates. This result agrees with the findings of Righi et al. (2016) and Unger (2011) who calculated a decrease of nitrate particles in the NH₃-limited mid-upper troposphere due to aircraft emissions and an increase in the lower troposphere and at surface. This is however in contrast to the results of Unger et al. (2013) who calculated an increase of NO₃ associated with aircraft emissions in most of the troposphere with a moderate 2-3% decrease in the upper-troposphere and lower-stratosphere, and consequently derived a strong negative forcing by nitrate particles as reported also by Brasseur et al. (2016). Please note that the impact of future climate change on aircraft perturbations is not considered in our simulations and should be investigated in forthcoming studies.

5.2 Mitigation scenarios

755 Two alternative future scenarios are derived from the future scenario QUANTIFY_A1. As described in Section 2, the QUANTIFY_LowNO_x scenario simulates the impact of NO_x emissions reduced by a factor 2, mimicking a significant improvement of the engine combustion technology with respect to NO_x emission index. The QUANTIFY_A1_Desulfurized scenario simulates the impact of a desulfurized fuel. In addition, two alternative scenarios representing two aircraft emission mitigation trajectories are used, these are the QUANTIFY_B1 and QUANTIFY_B1_ACARE scenarios described by Owen et al. (2010) and summarized in Section 2.

Figure 10 shows the impact of the LowNO_x and Desulfurized future emission scenarios on the zonal mean distribution of key atmospheric species. The low NO_x emissions have a significant impact on the ozone increase. In this case, the zonal mean ozone increase reaches a maximum of 5.9 ppbv in January (not shown) and 12 ppbv (8%) in May at 200 hPa. This corresponds to a reduction of 3 ppbv in January and 7 ppbv (40%) in May compared to the QUANTIFY_A1 scenario (**Fig. 9**). In this scenario, SO₄ is only moderately affected at flight altitude and the maximum SO₄ increase in May remains close to 33 ng/m³ (15%). However, in the lower troposphere, less sulfates are produced in the aqueous phase at lower O₃ concentrations especially in subsidence regions. The increase in SO₄ at the surface is significantly reduced and decrease from about 17 ng/m³ at 30°N in the QUANTIFY_A1 scenario to less than 10 ng/m³ in the QUANTIFY_LowNO_x simulation. In addition, as shown in **Fig. 10**, the impact on NO₃ is very limited at the flight cruise altitude. However, in the lower troposphere, the formation of nitrates through the reaction with NH₃ is decreased at lower NO_x emissions and the NO₃ concentration increase at the surface reaches 7 ng/m³ to be compared with the 14 ng/m³ calculated in the QUANTIFY_A1 simulation (**Fig. 9**). This is a factor of 2 reduction, linear with the decrease in total NO_x aircraft emissions in this scenario. This LowNO_x scenario has a significant impact on air quality reducing both tropospheric ozone but also the concentration of sulfates and nitrates in the lower troposphere.

In comparison to the QUANTIFY_A1 baseline scenario, the QUANTIFY_A1_Desulfurized simulation has, as expected, a significant impact on the SO₂ aircraft perturbation and consequently on the formation of SO₄. As seen from **Fig. 10**, since no emission of SO₂ and SO₄ are considered in this simulation, the SO₄ increase reaching 13 ng/m³ (5%) in May around 30°N and at 300-200 hPa is only associated with the increased production from SO₂ oxidation at higher ozone and OH concentrations. As a consequence of the reduced change in SO₄, a very moderate decrease in nitrates reaching only -6 ng/m³ (5%) is calculated at flight altitude. In the lower troposphere, the increase in NO₃ associated with production of ammonium nitrate from surface NH₃ emissions and aircraft NO_x reaches 14 ng/m³ (10%) as also calculated in the QUANTIFY_A1_Desulfurized scenario. These results agree with Unger (2011) and Kapadia et al. (2016) who calculated a similar impact of desulfurized fuel, a much lower increase of sulfates and nitrates at flight altitude and a significant increase in nitrates in the lower troposphere. As in Unger (2011), but in contrast to earlier work by Pitari et al. (2002), little effect of sulfate aerosols on ozone via heterogeneous chemistry is predicted in the upper troposphere. The impact of aircraft desulfurized fuel is close to the regular fuel ozone perturbation.

The results for the alternative economic and technological scenarios QUANTIFY_B1 and QUANTIFY_B1_ACARE (Owen et al., 2010) are illustrated in **Fig. 11**. QUANTIFY_B1 is a mitigation scenario for which improving air quality is a primary objective and therefore the reduction of NO_x, SO₂ and BC emissions are relatively important compared to the base case future scenario QUANTIFY_A1. In this case, as a consequence of lower NO_x emissions, the O₃ perturbation is reduced by more than a factor of 2 compared to QUANTIFY_A1 and the ozone zonal mean increase reaches a maximum of 4.5 ppbv in January (not shown) and of 8.6 ppbv (6%) in May compared to 9.2 ppbv and 19.6 ppbv in January and May, respectively, for the QUANTIFY_A1 simulation. For this mitigation scenario Hodnebrog et al. (2011) derived a model mean ozone increase at cruise altitude of 3 ppbv in January and about 5 ppbv in July, somewhat lower than our results. Again, it should be kept in mind that none of the models used in Hodnebrog et al. (2012) included an interactive chemistry in the stratosphere. The BC perturbation reaches a maximum of 0.35 ng/m³ (3%) at flight altitude, to be compared with 0.55 ng/m³ in the QUANTIFY_A1 simulation. The sulfate concentrations increase in May by up to 22 ng/m³ (9%) and as a consequence of this SO₄ increase, NO₃ are reduced by -14 ng/m³ (40%) at flight altitude, compared to 33 ng/m³ and -22 ng/m³, respectively, for the QUANTIFY_A1 scenario. The alternative scenario QUANTIFY_B1_ACARE is the most ambitious mitigation future scenario used in this study with very strong emission reductions. This scenario is an “extreme” scenario to limit the environmental impact of aviation. In this scenario, the NO_x emissions are reduced by almost a factor of 5 and the ozone increase reaches in May a maximum of 6.2 ppbv (4%), a value even lower than the ozone increase calculated under the QUANTIFY_2000 (6.8 ppbv) and REACT4C_2006 (6.4 ppbv) simulations. A significantly attenuated aerosol increase is also calculated for the QUANTIFY_B1_ACARE scenario, and BC and SO₄ increase by up to 0.25 ng/m³ (2%) and 16 ng/m³ (7%) at flight altitude respectively. The nitrate concentration decreases by 10 ng/m³ (30%) at flight altitude and increases by up to 3.8 ng/m³ (3%) in the lower troposphere (**Fig. 11**).

815 **6 Radiative forcing of climate**

6.1 Changes in ozone burden and methane lifetime

Table 4 summarizes the impact of aircraft emissions on the global burden of ozone and on the methane lifetime. Ozone increases by 4.7 Tg (0.430 DU) for the REACT4C_2006 reference scenario and an ozone production efficiency of 6.6 TgO₃/TgN is derived. The ozone sensitivity to aircraft NO_x emissions (0.6 DU/TgN) is similar to the adopted mean value reported by Holmes et al. (2011) (**Table S4**) and in the higher range of the 0.39-0.63 DU/TgN model range provided by Myhre et al. (2011). A somewhat higher values (0.79 DU/TgN for present-day conditions) was derived by Khodayari et al. (2014b) with the AEDT inventory. We note however that the ozone burden calculated by Koffi et al. (2010), presented in a model intercomparison by Hoor et al. (2009) (model mean of 5.6 TgO₃/TgN) and by Myrhe et al. (2011) were for global models including tropospheric chemistry solely. In

830 most of these earlier models (and in particular in an earlier 19 level version of LMDZ-INCA) the stratospheric
chemistry was not included and ozone constrained to climatologies above a potential temperature of 380 K. This
neglects the ozone change above the tropopause, as seen from **Fig. 5**. Olsen et al. (2013) derived a high model
spread for the ozone burden change per emitted NO_x of 2.5-11 TgO₃/TgN with some linearity of the model
835 responses to the NO_x emission. At higher flight altitudes (REACT4C_PLUS), the increase in ozone is about 15%
higher than for the reference case and at lower cruise altitude (REACT4C_MINUS) the increase in ozone is 11%
lower, reflecting longer NO_x residence time at higher altitude. This results in an increase in ozone production
efficiency reaching 7.5 at higher flight altitudes and a decrease to 5.8 at lower flight cruise altitude. In the case of
840 QUANTIFY_2000, the ozone burden increases by 5.0 Tg (0.457 DU) and the ozone production efficiency is
slightly lower (6.0) than for the REACT4C_2006 inventory, reflecting aircraft emissions deposited at somewhat
lower flight altitudes (Skowron et al., 2013). The reference present-day methane chemical lifetime calculated with
this model version is 10.6 yr, close to the present-day (2000) value reported by Voulgarakis et al. (2012) for a
previous version of the LMDZ-INCA model. Due to the increase in OH concentration when NO_x aircraft emissions
are considered, based on the REACT4C_2006 emission scenario, the methane chemical lifetime decreases by -
1.0% (-1.15% for the QUANTIFY_2000 aircraft emissions). A somewhat higher values (-1.65%/TgN for present-
day conditions) was derived by Khodayari et al. (2014b) with the AEDT inventory.

845 For the 2050 scenarios, ozone increases by up to 20.3 Tg (1.86 DU) for the QUANTIFY_A1 scenario and by 7-8
Tg (0.64-0.73 DU) for the B1 and B1_ACARE scenarios. Despite the very different atmospheric background in
2050, the derived ozone production efficiency for the A1 scenario (6.14) is rather close to the QUANTIFY_2000
reference value (6.0). A higher ozone production efficiency of respectively 7.7 and 7.9 is derived in the case of
the B1 and B1_ACARE scenarios. A similar feature was derived by Hodnebrog et al. (2011; 2012) for the
850 QUANTIFY inventories in 2050, with ozone production efficiencies averaged among several models (and for
different background conditions) of respectively 5.7, 7.4, 7.9 for the A1, B1 and B1_ACARE scenarios. For the
A1_LowNO_x scenario (future NO_x emissions reduced by 50%), the ozone burden decreases by 56% compared to
the A1 scenario, showing a very slight non-linearity. We calculate a methane reference lifetime in 2050 of 11.4
yr. Due to aircraft emissions, the future methane lifetime decreases by 4.7% for the QUANTIFY_A1 scenario and
855 by 1.8% and 1.2% for the B1 and B1_ACARE scenarios respectively. The calculated future ozone changes can
also be compared with more recent estimates involving global models including both tropospheric and
stratospheric chemistry. With the ACCRI_2050_Base and 2050-S1 emissions (**Table S2**), Olsen et al. (2013)
derived a global ozone burden increase ranging from 10.3 to 18.6 Tg (2.6-7.24 TgO₃/TgN) and from 4.5 to 13.8
Tg (2.9-8.8 TgO₃/TgN), respectively. More recently, Skowron et al. (2021) calculated with the MOZART-3 model
860 and based on a high (5.59 TgN) and a low (2.17 TgN) future (2050) aircraft emission scenarios, global ozone
increases of respectively 31 Tg and 15.4 Tg with some variation depending on the surface emission scenario,
providing respectively 5.5 TgO₃/TgN and 7.1 TgO₃/TgN. Our results agree with the ozone sensitivity to NO_x and
all these future simulations point to a decreasing ozone production efficiency at higher NO_x emissions. We again
stress that the impact of future climate change on aircraft perturbations is not considered in our simulations and
should be investigated in forthcoming studies.

865 **6.2 Radiative forcing from NO_x emissions**

The calculated radiative forcing of climate for the different scenarios are summarized in **Table 5**. The increase in
tropospheric ozone due to the aircraft NO_x emissions is responsible for a positive radiative forcing F_{O₃} of 15.9
870 mW/m² in the case of the reference scenario REACT4C_2006. This forcing increases by 1.85 mW/m² (12%) when
the flight altitude is increased in the case REACT4C_PLUS and decreases by 1.59 mW/m² (10%) when the flight
altitude is decreased in the case REACT4C_MINUS. In the case of QUANTIFY_2000 the calculated ozone
forcing is 17.2 mW/m², a value somewhat higher than REACT4C_2006 due to higher NO_x emissions. This value
agrees with the ozone forcings calculated by Hoor et al. (2009) in a multi-model study who derived a mean forcing
875 of 16.3 mW/m² for the QUANTIFY_2000 scenario. The calculated ozone forcing provides a forcing relative to
the NO_x emissions of 22.35 mW/m²/TgN. This value is in good agreement with Myhre et al. (2011) who calculated
a range for five models of 16-25 mW/m²/TgN and Holmes et al. (2011) who calculated based on factor
decomposition a forcing of 21.6 ± 7.2 mW/m²/TgN. As noted by Skowron et al. (2013), the ozone forcing is very
much dependent on the NO_x emission vertical profile with normalized forcings ranging from 16.5 to 20.5
880 mW/m²/TgN in their MOZART-3 simulations depending on the aircraft emission inventory considered. More
recently, Lee et al. (2021) derived a best estimate value of 25.1±7.2 mW/m²/TgN. As obtained by Holmes et al.
(2011), we derive an ozone forcing per DU of 37.1 mW/m²/DU, in agreement with this previous work (**Table S4**).
With different emission inventories, Olsen et al. (2013) reported an even wider range for the normalized ozone
forcing of 6-37 mW/m²/TgN. For the future scenarios, the tropospheric ozone forcing reaches 70.6 mW/m² for the
885 QUANTIFY_A1 scenario and 27.6 and 18.7 mW/m² in the case of the B1 and B1_ACARE mitigation scenarios,
respectively. These values agree with the ozone forcings calculated by Hodnebrog et al. (2011; 2012) in a multi-
model study who derived forcings of 61.3±14.0 mW/m², 24.1±7.7 mW/m² and 18.9±6.6 mW/m² for the
QUANTIFY_A1, QUANTIFY_B1 and B1_ACARE, respectively. For the reduced NO_x emission scenario
(A1_LowNO_x), the ozone forcing is 55% of the A1 scenario value, in line with the change in ozone burden.

890 The total methane forcing F_{CH₄} is broken down into four distinct forcings (**Table 6**). We calculate a direct radiative
forcing at equilibrium associated with the methane decrease F_{CH₄-OH} of -11.0 mW/m² for the “present-day”

895 REACT4C_2006 simulation (-12.5 mW/m^2 for the QUANTIFY_2000 simulation). For future conditions, the direct methane forcing ranges from -13.3 mW/m^2 for the QUANTIFY_B1_ACARE to -52.8 mW/m^2 for the QUANTIFY_A1 scenario. The indirect forcings associated with this change in methane mixing ratio through long-term tropospheric ozone ($F_{\text{CH}_4\text{-O}_3}$) and stratospheric water-vapour ($F_{\text{CH}_4\text{-SWV}}$) adjustments and calculated for the REACT4C_2006 simulation are respectively -2.82 mW/m^2 and -0.65 mW/m^2 (-3.30 mW/m^2 and -0.74 mW/m^2 , respectively, for the QUANTIFY_2000 simulation). For the future simulations we calculate an ozone long-term forcings $F_{\text{CH}_4\text{-O}_3}$ ranging from -3.6 mW/m^2 (B1_ACARE) to -13.96 mW/m^2 (A1) and a stratospheric water vapour forcings $F_{\text{CH}_4\text{-SWV}}$ ranging from -0.82 mW/m^2 (B1_ACARE) to -3.22 mW/m^2 (A1). The indirect radiative forcings from CO_2 production ($F_{\text{CH}_4\text{-CO}_2}$) are -0.20 mW/m^2 and -0.23 mW/m^2 for the “present-day” simulations REACT4C_2006 and QUANTIFY_2000, respectively, and range from -0.21 mW/m^2 (B1_ACARE) to -0.81 mW/m^2 (A1) in 2050. The sum of these four components provides F_{CH_4} the total methane radiative forcing associated with aircraft NO_x emissions. This total forcing is -14.7 mW/m^2 and -16.7 mW/m^2 for the “present-day” REACT4C_2004 and QUANTIFY_2000 inventories, respectively. In 2050, the total methane forcing ranges from -17.9 mW/m^2 for QUANTIFY_B1_ACARE to -70.8 mW/m^2 for the A1 scenario (**Table 6**). The change in CH_4 mixing ratio itself represents 75% of this total methane forcing. The indirect changes through long-term tropospheric ozone, stratospheric water vapour and oxidation to CO_2 contribute for 19%, 4% and 1%, respectively.

910 As seen in **Table 5**, the NO_x forcing components resulting from the tropospheric ozone positive forcing and the methane negative forcing largely offset each other resulting in a slightly positive forcing of 1.2 and 0.5 mW/m^2 for the REACT4C_2006 and QUANTIFY_2000 “present-day” simulations. In 2050, a net negative forcing of -0.28 mW/m^2 is calculated for the QUANTIFY_A1 scenario. For the alternative scenarios B1 and B1_ACARE we still derive positive forcings of 1.14 and 0.84 mW/m^2 . This partial compensation and the resulting positive or negative NO_x net forcing depends on the level of NO_x present in the background atmosphere and the location of emissions (Stevenson and Derwent, 2009; Gilmore et al., 2013; Skowron et al., 2021). Thus, for the future, higher concentrations of NO_x increase the OH response and the effect of methane so that total NO_x forcings even become negative. **Table S3** compares the methane forcings calculated with the revised CH_4 radiative forcing parameterization proposed by Etminan et al. (2016) and by the former parameterization (Myhre et al., 1998). The net NO_x negative forcings calculated for future conditions in this study are largely affected by this methane forcing parameterization. $F_{\text{CH}_4\text{-OH}}$ is higher by 23% when Etminan et al. (2016) parameterization is used and the total methane forcing is higher by about 15%. In the case of the methane forcing former parameterization (Myhre et al., 1998), positive NO_x net forcings ranging from $3.3\text{-}5.0 \text{ mW/m}^2$ for “present-day” conditions to $3.3\text{-}9.7 \text{ mW/m}^2$ in 2050 are calculated. A similar conclusion regarding the possibility to have negative NO_x net forcings has been reached by Skowron et al. (2021). The radiative forcings associated with NO_x emissions are decomposed into its various factors following Holmes et al. (2011) methodology, and compared to previous estimates at **Table S4**. A good agreement is found for the various components or sensitivities of the chemistry and of the radiative forcings with the previous estimate provided by Holmes et al. (2011). The major difference arises from the methane forcing calculation based on Etminan et al. (2016) in our study. Similarly, the forcings normalized by emissions are also generally in agreement with Lee et al. (2021).

935 The sensitivity of the NO_x associated forcings with aircraft flight altitude has been investigated in earlier studies (Gauss et al., 2006; Frömming et al., 2012; Søvde et al., 2014). In particular, based on the REACT4C emission inventories, Søvde et al. (2014) derived, in a multi-model study, an increase of the total NO_x forcing of $2\pm 1 \text{ mW/m}^2$ for aircraft cruising at higher altitudes and a decrease of the forcing by the same value for aircraft cruising at lower altitudes with a change essentially due to the ozone forcing. In this study, the NO_x net forcing is increased by 1.74 mW/m^2 for aircraft cruising at higher altitudes and decreased by 1.58 mW/m^2 at lower altitudes. These values agree with this previous estimate. It should be noticed that based on the Etminan et al. (2016) parameterization, the NO_x net forcing turns from positive to negative when the aircraft cruise altitude is reduced (**Table S3**).

940 As illustrated by the REACT4C_2006_NOx_Only simulation results (only the NO_x emissions are perturbed by aviation without including the other chemical and aerosol emissions) shown in **Table 5** and **Tables S4**, additional forcings arise from aircraft NO_x emissions. This sensitivity simulation shows that the change in OH associated with NO_x emissions is responsible for an increased formation of sulfate particles and a negative forcing from these aerosols of -2.0 mW/m^2 . Similarly, NO_x emissions and concentrations increase the formation of nitrate particles, also responsible for an additional negative forcing of -0.12 mW/m^2 . The nitrate forcing calculated by Pitari et al. (2016) is much higher (-1.7 mW/m^2) but the role played by ammonia was not considered in this earlier study. The ammonium cycle is important to consider since we discussed earlier that in the lower troposphere increased NO_x from aircraft emissions increase nitrates particles. However, in the upper troposphere, increased sulfate concentrations will favor the titration of ammonia to form ammonium sulfates leading to lower ammonium nitrate concentrations despite the increased NO_x and HNO_3 concentrations. The total forcing of sulfate and nitrate aerosols associated with NO_x emissions is -2.12 mW/m^2 . When these aerosol direct radiative forcings are considered, the total net NO_x forcing switches from a positive value of 1.19 mW/m^2 from tropospheric ozone plus methane to -0.93 mW/m^2 . When these indirect terms are accounted for, we derive a negative net NO_x radiative forcing per TgN emitted by aviation as summarized in **Table S4**. Including the forcings associated with particles (SO_4 and NO_3) is found to change the sign of the next NO_x radiative forcings compared to the earlier studies of Holmes et al. (2011) and Lee et al. (2021). It should be kept in mind that the forcings associated with aerosols are of course subject to

large uncertainties in the models (Lee et al., 2021; Forster et al., 2021) and more model simulations are needed in order to gain more confidence in these results.

960

It should also be noted that these two forcings from ozone and methane represent perturbations at steady-state. This assumption is correct for tropospheric ozone which has an averaged of a few weeks but is not for methane which has lifetime of 10.6 years in our model. For methane, the response does not reach a steady-state in any given year and the response in a particular year depends on the historical time-evolving emissions. This limitation was for instance discussed and illustrated by Khodayari et al. (2014b), Grewe et al. (2019), Lee et al. (2021) and Matthes et al. (2021). For this reason, a transient correction factor was applied to the total methane forcing by Myhre et al. (2011), Hodnebrog et al. (2011; 2012), Matthes et al. (2021) and in the best estimate provided by Lee et al. (2021). However, this factor has not been considered in Brasseur et al. (2016) or, more recently, in Skowron et al. (2021). The major difficulty with this non-steady state factor is that its determination is strongly model dependent. Due to the long time-integration needed to investigate the methane response, complex models have not been used so far and the non-steady state factor has been determined based on simplified or parameterized chemistry-climate models (Grewe and Stenke, 2008; Lee et al., 2021). Another difficulty in determining this factor, and in particular for future scenarios, arises from its dependency on the considered year or on the assumed future emission pathway. For the QUANTIFY_2000 emissions, Myhre et al. (2011) derived, based on Grewe and Stenke (2008) methodology, a non-steady state correction factor of 0.65. A similar factor has been used by Matthes et al. (2021). This factor has been recently reassessed by Lee et al. (2021) with a two-dimensional model and a factor of 0.73 and 0.79 were determined for 2000 and 2018, respectively. For the future 2050 scenarios, Hodnebrog et al. (2011; 2012) derived factors of 0.74, 1.0, and 1.15 for the QUANTIFY A1B, B1 and B1_ACARE, respectively. Considering the uncertainty associated with this factor, the forcings calculated in this study assumed a steady-state methane perturbation, as was done by Skowron et al. (2021). However, for sake of completeness, **Table S5** compares the standard steady-state forcings and the forcings with non-steady factors applied. The factors provided by Lee et al. (2021) for the 2000 and 2005 simulations and by Hodnebrog et al. (2011; 2012) for the 2050 scenarios have been used. When these non-steady methane forcings are considered, the future NO_x net forcings are generally higher and even switch back to positive in 2050. We note however the high uncertainty on these factors and the need for future work in order to provide a more robust estimate of this non-steady state correction and overall methodology.

965

970

975

980

985

6.3 Direct radiative forcing from SO₂ and particulate carbon emissions

990

The concentrations of several types of particles are perturbed by aircraft emissions and hence provide direct radiative forcings (**Table 5**). Direct emissions of soot particles induce a positive radiative forcing of 0.46 mW/m² in the case of the REACT4C_2006 inventory and 0.54 mW/m² for the QUANTIFY_2000 inventory. With the REACT4C inventory, Pitari et al. (2015) calculated a higher direct soot forcing of 0.78 mW/m². We note however that the soot radiative forcing is subject to large uncertainties. In 2050, this forcing reaches 1.88 mW/m² for the QUANTIFY_A1 scenario. For these particles we derive a normalized forcing of 108-115 mW/m²/Tg for present-day conditions, in the range provided by Balkanski et al. (2010) of 8-140 mW/m²/Tg and calculated based on the QUANTIFY emissions. The calculated normalized forcing is also in good agreement with the recent study of Brasseur et al. (2016) providing a range of 101-168 mW/m²/Tg.

995

1000

Sulfates particle concentrations are also perturbed by the aviation SO₂ emissions and by the direct SO₄ emissions. The negative forcing associated with an increase of these particles largely dominates the effect of the other particles and ranges from -3.87 mW/m² and -4.33 mW/m² for the REACT4C_2006 and QUANTIFY_2000 “present-day” simulations to -13.7 mW/m² in 2050 under the QUANTIFY_A1 scenario. With the REACT4C inventory, Pitari et al. (2015) calculated a direct sulfate forcing of -3.5 mW/m², a value close to this study. For these particles we derive a normalized direct forcing of -52.8 (REACT4C_2006) and -49.3 (QUANTIFY_2000) mW/m²/TgS for “present-day” conditions, in the range provided by Unger (2011) of -56 mW/m²/TgS and Brasseur et al. (2016) of -27/-62 mW/m²/TgS. The atmospheric distribution of ammonium nitrate particles is indirectly affected by aviation emissions and dominated by the increase in sulfates favoring the formation of ammonium sulfates over ammonium nitrates. The decrease in nitrate particles is responsible for a positive forcing ranging from 0.07 mW/m² for the “present-day” to 1.3 mW/m² in 2050 for the A1 scenario. The impact of aircraft emissions on nitrates very much depends on the NH₃ and SO₂ levels in the upper troposphere as discussed by Unger et al. (2013) who calculated a much larger nitrate forcing from aircraft in their future simulations. The results of LMDZ-INCA showed a good comparison with other models as illustrated by the model intercomparison presented by Bian et al. (2017). A slight negative forcing reaching -0.16 mW/m² in 2050 is associated with the emission of organic carbon by aviation. In total, aerosols are responsible for a negative direct forcing largely dominated by sulfate particles and ranging from -3.4 mW/m² in the case of REACT4C_2006 to -10.6 mW/m² in 2050 for the A1 scenario.

1005

1010

1015

1020

The variation of aircraft flight altitude modifies the residence time of particles in the atmosphere. A longer life time is associated with a higher injection altitude and therefore influences concentration changes and the radiative forcing associated with these particles. The forcing associated with soot particles increases from 0.46 mW/m² in the case of the REACT4C_2006 scenario to 0.49 mW/m² at higher flight altitudes and decreases to 0.44 mW/m² at lower altitudes. The dominant forcing from aviation-induced particles remains the negative forcing from sulfates. This forcing decreases from -3.87 mW/m² to -4.38 mW/m² at higher flight altitudes and increases to -

1025 3.40 mW/m² at lower altitudes. The total aerosol forcing is dominated by sulfates and its variation with flight altitude reflects the variation of the sulfate negative forcing. The total aerosol direct forcing decreases by to -3.0 mW/m² (-12%) at lower flight altitudes (REACT4C_MINUS) and increases to -3.8 mW/m² (+13%) at higher flight altitudes (REACT4C_PLUS).

1030 For the future QUANTIFY_A1 simulation, the use of desulfurized fuel reduces the sulfate direct forcing by 55%. The remaining sulfate forcing is associated with changes in OH and increased sulfate formation. However, the reduced direct SO₂ (and SO₄) emissions have the consequence to decrease the sulfate forcing to -6.5 mW/m². The use of desulfurized fuel also has an impact on nitrates particles. In this case, the nitrates are essentially affected by increased NO_x concentrations and a negative forcing of -0.8 mW/m² is calculated. In total, the use of desulfurized fuel decreases the forcing of particles from -12.4 mW/m² to -5.6 mW/m². The ozone forcing is only slightly affected by the removal of SO₂ aircraft emissions in agreement with Unger (2011).

6.4 Radiative forcing from water vapour emissions

1040 The radiative forcing associated with water vapour increase in the stratosphere due to direct aircraft emissions and calculated with the LMDZ-INCA model is 0.13-0.16 mW/m² for “present-day” conditions (REACT4C_2006 and QUANTIFY_2000) and increases to 0.52 mW/m² in 2050 under the QUANTIFY_A1 scenario (**Table 5**). Based on earlier literature, Lee et al. (2009) reported a best estimate for this forcing of 2.8 mW/m² with a range of 0.39-20.3 mW/m². More recently Lee et al. (2021) reported values ranging from 0.4 mW/m² (Wilcox et al., 2012) to 1.5 mW/m² (Fromming et al., 2012; Lim et al., 2015) and even to 3.0 mW/m² (Penner et al., 2009), and derived a best estimate for this forcing of 2.0 (0.8, 3.2) mW/m². The forcing recalculated with the LMDZ-INCA chemistry-transport model is at the lower range of this previous literature.

1050 Myhre et al. (2009) performed an intercomparison of stratospheric water vapour radiative forcings from several models imposing idealized stratospheric H₂O perturbations. In particular, a simulation imposing an increase of water vapour in the stratosphere from 3 to 3.7 ppmv has been performed. In this case, based on 6 different models the calculated net radiative forcings at the tropopause ranged from 0.16 to 0.38 W/m² with a mean at 0.25 W/m². The longwave forcings range from 0.19 to 0.40 W/m² and the shortwave forcings range from -0.020 to -0.058 W/m². In order to evaluate our radiative transfer model, we have performed this benchmark simulation with the LMDZ-INCA model version used in the present study. We calculate a net radiative forcing at the tropopause of 0.18 W/m² (longwave: 0.22 W/m²; shortwave: -0.038 W/m²). These forcings agree with the model ranges provided by Myhre et al. (2009) for both forcing components.

1060 The water vapour forcing associated with aircraft emissions calculated in this study is based on a detailed calculation involving stratospheric chemistry and transport and includes only the water vapour change above the tropopause. This forcing is at the lower range of previous estimates. It should be noted that these previous estimates are based on different model set-up. For instance, Wilcox et al. (2012) used a Lagrangian model for transport imposing a water vapour lifetime and Frömming et al. (2012) provided a water vapour forcing including both the H₂O change in the stratosphere and upper troposphere. In Brasseur et al. (2016), the reported stratospheric water vapour forcings by two models (1.3 and 2.0 mW/m²) did account for both direct H₂O emissions and photochemical production by methane. A more detailed evaluation of this stratospheric water vapour forcing associated with direct aircraft emissions is still needed based on various models using the same protocol for calculation.

6.5 Total direct radiative forcing from atmospheric composition changes

1070 The total radiative forcing from aircraft emissions and associated with changes in atmospheric chemistry and direct aerosols forcings are given in **Table 5**. The total forcing calculated with the LMDZ-INCA model are negative for both the “present-day” and future (2050) simulations. The total forcing ranges from -2.1 mW/m² for the “present-day” inventory REACT4C_2006 (-3.1 mW/m² in the case of the QUANTIFY_2000 inventory) to -2.5 mW/m² in 2050 for the QUANTIFY_B1_ACARE scenario and to -10.4 mW/m² for the QUANTIFY_A1 scenario. A total negative forcing from reactive species and aerosol direct forcings was also calculated by Unger et al. (2013) for both present and future conditions based on the AEDT emission inventories. The total forcing associated with NO_x only emissions (REACT4C_2006_NOx_Only) also becomes negative (-0.93 mW/m²) when the indirect forcings from sulfates and nitrates particles are considered. The comparison with the baseline simulation (REACT4C_2006) indicates that the climate effect of NO_x emissions amounts to about 45% of the total perturbation. In the future simulations, this translates into a decrease of the total forcing by about 30% when the NO_x emissions are reduced by 50%. Since sulfates dominate the particulate radiative forcing from aircraft, lowering the fuel sulfur content is another potential mitigation option to reduce the total forcing. For the future QUANTIFY_A1 simulation, the use of desulfurized fuel reduces the total forcing by more than 45%.

1085 The net effect of decreasing the flight cruise altitude by 2000 ft is to increase the total negative forcing from -2 mW/m² to -3.2 mW/m² (+57%). Increasing the flight altitude by 2000 ft decreases the negative forcing to -0.7 mW/m² (-65%). The variation of the total forcing with flight altitude is dominated by the high sensitivity of the ozone positive forcing to the altitude of the perturbation, with the variation of the negative sulfate forcing of secondary importance for these sensitivity simulations.

1090

The Radiative Forcings (RF) and Effective Radiative Forcings (ERFs) from aircraft emissions calculated in this study are compared to the recent review by Lee et al. (2021) at **Table 7**. For this comparison the forcings are scaled to the 2018 aircraft fuel and the ERF/RF ratios provided by Lee et al. (2021) are applied to derive the ERF. For the methane forcing, we also apply the transient correction factor (see **Section 6.2**) recalculated and applied by Lee et al. (2021) for the best estimates (0.79). Overall, the agreement for the total forcing between this study and the best estimate from Lee et al. (2021) and based on the previous literature is reasonable. However, a detailed comparison shows that both the ozone positive and methane negative forcings are lower in LMDZ-INCA compared to the Lee et al. (2021) assessment, but remain in the 5-95% uncertainty range provided in that study. The ozone forcing calculated in this study is in better agreement with the Holmes et al. (2011) best estimate as discussed earlier (see also **Table S4**). As indicated above the stratospheric water vapour forcing is also significantly lower and requires further attention. It is also important to note that the total ERF is now positive and equal to 8.9 mW/m² (comparing well with the 8.6 mW/m² best estimate from Lee et al. (2021)). while the total radiative forcing calculated in **Table 5** was negative (-2.06 mW/m²). This is due to the increase, in Lee et al. (2021), of the ozone ERF by almost 40% compared to the radiative forcing while keeping the aerosol forcings unchanged (ERF/RF = 1). Considering the uncertainty on the determination of the ERF/RF ratio for the different forcing agents, which depends on the climate model used, this feature also clearly requires further investigation. A similar conclusion applies to the methane transient factor estimate.

1095

1100

1105

7 Summary and conclusion

1110

Aviation NO_x emissions have not only an impact on global climate by changing ozone and methane levels in the atmosphere but also contribute to deteriorate local air quality. Improved combustor performance from future aircraft can therefore contribute to reduce the impact of aircraft on climate but also provide a co-beneficial improvement of air quality. However, historically, reductions in aircraft NO_x emissions have tended to increase fuel burn and hence CO₂ emissions. Thus, a trade-off generally arises between reducing aircraft NO_x and CO₂ emissions. In order to properly assess the co-benefit with air quality improvement and the trade-off with climate change due to CO₂ emissions, it appears essential to better quantify the climate impact of aircraft NO_x emissions and its future evolution.

1115

1120

In this paper, a new version of the LMDZ-INCA global model is applied to re-evaluate the impact of aircraft NO_x and aerosol emissions on climate. This version of the model is better designed to investigate the role played by aircraft emissions in the upper-troposphere and lower-stratosphere and includes both the gas phase chemistry in the troposphere and in the stratosphere. The model results have been compared to ozone soundings and to IAGOS data for O₃ and CO in the upper-troposphere and lower-stratosphere. In addition, tropospheric aerosols are also considered including the sulfate-nitrate-ammonium cycle and heterogeneous reactions between gas phase chemistry and aerosols. With this model, we investigate the impact of “present-day” baseline and future (2050) aircraft emissions on atmospheric composition and the associated radiative forcings of climate of ozone, methane and the aerosol direct forcings.

1125

1130

The key results from this study can be summarized as follows:

1. The results from the various simulations performed in this study confirm that the efficiency of NO_x to produce ozone is very much dependent on the cruise altitude. Flying higher increases the impact of NO_x on ozone and flying lower reduces the impact on ozone. In the future, an ozone production four times higher than for the “present-day” is calculated. An increase roughly linear with the increase in NO_x emissions. The future evolution of the ozone production efficiency indicates that this efficiency increases with the background methane and NO_x concentrations. The efficiency also increases with decreasing aircraft NO_x emissions.

1135

2. As a result of NO_x aircraft emissions, the atmospheric methane sink is decreased by about 1% for the “present-day” simulations and by up to 4.7% in 2050. We found the methane lifetime variation is less sensitive to the aircraft NO_x emission location than the ozone change. Similarly, the methane sink appears slightly less sensitive than the ozone production to the amount of aircraft NO_x emitted. This agrees with Holmes et al. (2011) and Skowron et al. (2021) who found ozone more responsive to aircraft emissions than methane. The net NO_x forcing (O₃ + CH₄) is largely affected by the revised CH₄ radiative forcing formula provided by Etminan et al. (2016) which increases by 15% the total CH₄ negative forcing. As a consequence, the ozone positive forcing and the methane negative forcing largely offset each other resulting in a slightly positive forcing for “present-day” simulations. In 2050, the net forcing even turns negative due essentially to higher methane background concentrations. Skowron et al. (2021) also reached the similar conclusion that the revision of the methane radiative forcing significantly reduced the aircraft NO_x forcing and that, in the future, this forcing could even turn negative, providing a different perspective on the aircraft NO_x emissions impact on climate.

1140

1145

1150

3. Additional radiative forcings involving particle formation arise from aircraft NO_x emissions and the sulfate-nitrate-ammonium cycle is also important to consider. The increased OH concentrations associated with NO_x emissions are responsible for an enhanced conversion of SO₂ to sulfate particles and an associated negative forcing. NO_x emissions from aircraft also increase nitrates particles in the lower troposphere where ammonia

1155

concentration are higher. In the upper troposphere, increased sulfate concentrations favor the titration of ammonia to form ammonium sulfates leading to lower ammonium nitrate concentrations (despite the increased NO_x and HNO_3 concentrations). Overall, the indirect forcings of sulfate and nitrate aerosols associated with NO_x emissions is negative and is estimated to $-3.0 \text{ mW/m}^2/\text{TgN}$. When these aerosol radiative forcings are considered, the net NO_x forcing, due to O_3 and CH_4 , and estimated to $+2 \text{ mW/m}^2/\text{TgN}$, turns from a positive value to a negative value even for present-day conditions. The aerosol indirect forcings are subject to large uncertainties and are in particular sensitive to the model sulfate-ammonium-nitrate scheme (Unger et al., 2011; Righi et al., 2013; Pitari et al., 2016; Brasseur et al., 2016). Further investigation is clearly needed in order to gain more insight into these aircraft indirect forcings. Despite these uncertainties the results suggest that, in addition to the increased methane negative forcing discussed above, indirect forcing from sulfate and nitrate particles could turn the aircraft NO_x radiative forcing from positive to negative even for present-day conditions and not only under future scenarios.

4. The concentrations of several types of particles are perturbed by aircraft emissions and hence provide direct radiative forcings of climate. The negative forcing associated with sulfates largely dominates the effect of the other particles. The sulfate direct radiative forcing is estimated to be associated for about 50% to the direct SO_2 and SO_4 aircraft emissions and for about 50% to the increased conversion of SO_2 to SO_4 at higher OH concentrations, and hence related to the NO_x emissions. In the future, the use of desulfurized fuel reduces the sulfate direct forcing and also has an impact on nitrates particles. Lowering the fuel sulfur content is hence a potential mitigation option to reduce this aircraft negative forcing by more than 45%. We found the ozone forcing only slightly affected by heterogeneous chemistry in the upper-troposphere.

5. The radiative forcing associated with direct aircraft emissions of water vapour in the stratosphere is calculated in this study based on a detailed calculation involving stratospheric chemistry and transport and include only the water vapour change above the tropopause. This forcing is at the lower range of previous estimates. It should be noted that these previous estimates are based on very different model set-up. This forcing is likely to be small, however, a more detailed evaluation of this stratospheric water vapour forcing associated with direct aircraft emissions is still needed based on several models using the same protocol for calculation.

6. Overall, the agreement for the non- CO_2 total forcing between this study and the best estimate from Lee et al. (2021) is reasonable. However, a detailed comparison reveals several key differences and points to the key uncertainties associated with the NO_x and aerosol direct forcings. Both the ozone positive and methane negative forcings are lower in LMDZ-INCA compared to the Lee et al. (2021) assessment, while remaining in the 5-95% confidence range. This is mostly due to the increase, in Lee et al. (2021), of the ozone ERF by almost 40% compared to the radiative forcing while keeping the aerosol forcings unchanged (ERF/RF = 1). Considering the uncertainty on the determination of the ERF/RF ratio for the different forcing agents, which depends on the climate model used, this feature clearly requires further investigation. A similar conclusion applies to the methane transient factor estimate which can flip the sign of the total NO_x forcing.

7. Several previous studies have suggested that cruise emissions could be a significant or even dominant contribution to aviation-attributable surface level particulate matter and ozone (e.g., Barrett et al., 2010; Unger, 2011; Hauglustaine and Koffi, 2012; Lee et al., 2013; Eastham and Barrett, 2016). Our results confirm this important subsidence of ozone produced in the free troposphere by cruise altitude NO_x emissions, down to the lower troposphere and surface. A similar downward transport of black carbon and sulfates is also simulated by the global model with a significant increase of particulate matter levels at the surface. We further find that aircraft NO_x emissions are responsible, in the lower troposphere, for an important formation of ammonium nitrate particles, in particular in regions of high ammonia concentrations. Since ammonia concentrations are predicted to increase in the future (Hauglustaine et al., 2014), the aircraft NO_x emissions could become a significant source of nitrate particles near the ground, in addition to contributing already significantly to ground-level sulfates and ozone concentrations.

These results show that several mitigation options involving aircraft flight operation and cruise altitude changes, traffic growth, engine technology, and fuel type, exist to reduce the climate impact of aircraft NO_x emissions. However, our results, based on a current state-of-the-art global model, also show that the climate forcing of aircraft NO_x emissions is likely to be small or even turn to negative (cooling) depending on atmospheric NO_x or CH_4 future background concentrations and when the aircraft NO_x impact on sulfate and nitrate particles is considered. Following previous work methodology, in order to better emphasize the impact of aircraft emissions on atmospheric composition, the impact of future climate change on aircraft perturbations is not considered in our simulations performed based on a present-day, unchanged, meteorology in 2050. The simulations performed by Oliv   et al. (2012) and Huszar et al. (2013) did account for future climate change, however, the impact of future climate on atmospheric composition changes due to aircraft emissions is not isolated. Changes in upper-tropospheric temperature, humidity, and dynamics have the potential to affect the response of the atmosphere to aircraft emissions. These perturbations are likely to be more pronounced at a longer time-horizon than at the 2050 timeframe considered in our simulations, but this topic is clearly a subject to be investigated in forthcoming studies. There are still large uncertainties on the estimate of the aircraft NO_x net impact on climate. In particular the use of Effective Radiative Forcings (ERFs) or accounting for the methane transient forcing varies among the different models. These methodological concepts also require further investigation in order to determine the best appropriate

metric to express the climate impact of aircraft NO_x. There remain large uncertainties on the NO_x net impact on climate and in particular on the indirect forcings associated with aerosols which are even more uncertain than the other forcings from gaseous species. Additional studies with a range of models are hence needed in order to provide a more consolidated view. Nevertheless, the results seem to suggest that reducing aircraft NO_x emissions is primarily beneficial for improving air quality and reducing O₃ and Particulate Matter (PM) ground-level concentrations. New technologies in combustor design, which could help to reduce simultaneously NO_x and CO₂ emissions, do not appear essential for aircraft non-CO₂ climate mitigation but rather as being co-beneficial for climate change mitigation from CO₂ emission reduction and for air quality improvement from reduced aviation NO_x emissions.

Acknowledgements. We thank Yunjiang Zhang for preparing the model Aerosol Optical Depth evaluation against MODIS and AERONET data. This study was partly funded by the Direction Générale de l'Aviation Civile (DGAC) under the IMPACT and CLIMAVIATION projects and by the European Union Horizon 2020 research and innovation programme under the ACACIA project (Grant Agreement No 875036). The simulations were performed using HPC resources from GENCI (Grand Equipement National de Calcul Intensif).

References

- 1240 Balkanski, Y., Myhre, G., Gauss, M., Rädel, G., Highwood, E. J., and Shine, K. P.: Direct radiative effect of aerosols emitted by transport: from road, shipping and aviation, *Atmos. Chem. Phys.*, 10, 4477-4489, doi:10.5194/acp-10-4477-2010, 2010.
- Barrett, S.R.H. Rex E. Britter and Ian A. Waitz, Global mortality attributable to aircraft cruise emissions. *Environmental Science and Technology* 44 (19), pp. 7736-7742. DOI: 10.1021/es101325r, 2010.
- 1245 Bauer, S., Y. Balkanski, M. Schulz, D. A. Hauglustaine, et F. Dentener, Heterogeneous chemistry on mineral aerosol surfaces: a global modelling study on the influence on tropospheric ozone chemistry and comparison to observations, *J. Geophys. Res.*, 109, D02304, doi:10.1029/2003JD003868, 2004.
- 1250 Berntsen, T. K., J. S. Fuglestedt, M. Joshi, K. P. Shine, N. Stuber, M. Ponater, R. Sausen, D. A. Hauglustaine, and L. Li, Climate response to regional emissions of ozone precursors; sensitivities and warming potentials, *Tellus B*, 57, 283-304, 2005.
- Bian, H., Chin, M., Hauglustaine, D. A., Schulz, M., Myhre, G., Bauer, S. E., Lund, M. T., Karydis, V. A., Kucsera, T. L., Pan, X., Pozzer, A., Skeie, R. B., Steenrod, S. D., Sudo, K., Tsigaridis, K., Tsimpidi, A. P., and Tsyro, S. G.: Investigation of global particulate nitrate from the AeroCom phase III experiment, *Atmos. Chem. Phys.*, 17, 12911–12940, <https://doi.org/10.5194/acp-17-12911-2017>, 2017.
- 1255 Boucher, O., P. Friedlingstein, B. Collins, and K. P. Shine, The indirect global warming potential and global temperature change potential due to methane oxidation, *Environmental Research Letters*, 4, 4, 2009.
- Boucher, O., Servonnat, J., Albright, A. L., Aumont, O., Balkanski, Y., & Bastrikov, V. et al. (2020). Presentation and evaluation of the IPSL - CM6A - LR climate model. *Journal of Advances in Modeling Earth Systems*, 12, e2019MS002010. <https://doi.org/10.1029/2019MS002010>, 2020.
- 1260 Boucher, O., A. Borella, T. Gasser and D. Hauglustaine, On the contribution of global aviation to the CO₂ radiative forcing of climate, *Atmos. Environ.*, 267, 2021.
- Bousquet, P., C. Yver, I. Pison, Y. S. Li, A. Fortems, D. Hauglustaine, S. Szopa, P. J. Rayner, P. Novelli, R. Langenfelds, P. Steele, M. Ramonet, M. Schmidt, P. Foster, C. Morfopulos, et P. Ciais, A 3D synthesis inversion of the molecular hydrogen cycle: sources and sinks budget implications for the soil uptake, *J. Geophys. Res.*, 116, D01302, 2010.
- Bouwman, A. F., D. S. Lee, W. A. H. Asman, F. J. Dentener, K. W. Van Der Hoek, and J. G. J. Olivier, A global high-resolution emission inventory for ammonia, *Global Biogeochem. Cycles*, 11, 561-587, 1997.
- 1270 Brasseur G. P., R. A. Cox, D. A. Hauglustaine, I. Isaksen, J. Lelieveld, D. H. Lister, R. Sausen, U. Schumann, A. Wahner et P. Wiesen, European scientific assessment of the atmospheric effects of aircraft emissions, *Atmos. Environ.*, 32, 2329-2418, 1998.
- Brasseur, G. P., et al., Impact of aviation on climate, *Bulletin of the American Meteorological Society*, 97(4), 561-583, 2016.
- 1275 Brunner, D., J. Staehelin, H. L. Rogers, M. O. Köhler, J. A. Pyle, D. A. Hauglustaine, L. Jourdain, T. K. Berntsen, M. Gauss, I. S. A. Isaksen, E. Meijer, P. van Velthoven, G. Pitari, E. Mancini, V. Grewe, et R. Sausen, An evaluation of the performance of chemistry transport models by comparison with research aircraft observations. Part 1: concepts and overall model performance, *Atmos. Chem. Phys.*, 3, 1606-1631, 2003.
- Brunner, D., J. Staehelin, H. L. Rodgers, M. O. Kohler, J. A. Pyle, D. A. Hauglustaine, L. Jourdain, T. K. Berntsen, M. Gauss, I. S. A. Isaksen, E. Meijer, P. van Velthoven, G. Pitari, E. Mancini, V. Grewe, et R. Sausen, An evaluation of the performance of chemistry transport models. Part 2: detailed comparison with two selected campaigns, *Atmos. Chem. Phys.*, 5, 107-129, 2005.
- 1280 Cameron, M.A., Jacobson, M.Z., Barrett, S.R.H., Bian, H., Chen, C.C., Eastham, S.D., Gettelman, A., Khodayari, A., Liang, Q., Selkirk, H.B., Unger, N., Wuebbles, D.J., Yue, X., An intercomparative study of the effects of aircraft emissions on surface air quality. *J. Geophys. Res.* 122, 8325–8344. doi:10.1002/2016JD025594, 2017.
- 1285 Carslaw, K., Luo, B., and Peter, T.: An analytic expression for the composite of aqueous HNO₃-H₂SO₄ stratospheric aerosols including gas phase removal of HNO₃, *Geophys. Res. Lett.*, 22, 18771880, 1995.
- Clappier, A., Belis, C. A., Pernigotti, D., and Thunis, P.: Source apportionment and sensitivity analysis: two methodologies with two different purposes, *Geosci. Model Dev.*, 10, 4245–4256, <https://doi.org/10.5194/gmd-10-4245-2017>, 2017.
- 1290 Cohen, Y., Petetin, H., Thouret, V., Marécal, V., Josse, B., Clark, H., Sauvage, B., Fontaine, A., Athier, G., Blot, R., Boulanger, D., Cousin, J.-M., and Nédélec, P.: Climatology and long-term evolution of ozone and carbon monoxide in the upper troposphere–lower stratosphere (UTLS) at northern midlatitudes, as seen by IAGOS from 1995 to 2013, *Atmos. Chem. Phys.*, 18, 5415–5453, <https://doi.org/10.5194/acp-18-5415-2018>, 2018.
- 1295 Cohen, Y., Marécal, V., Josse, B., and Thouret, V.: Interpol-IAGOS: a new method for assessing long-term chemistry–climate simulations in the UTLS based on IAGOS data, and its application to the MOCAGE CCM1 REF-C1SD simulation, *Geosci. Model Dev.*, 14, 2659–2689, doi:10.5194/gmd-14-2659-2021, 2021.
- 1300 Collins, W. J., Lamarque, J.-F., Schulz, M., Boucher, O., Eyring, V., Hegglin, M. I., Maycock, A., Myhre, G., Prather, M., Shindell, D., and Smith, S. J.: AerChemMIP: quantifying the effects of chemistry and aerosols in CMIP6, *Geosci. Model Dev.*, 10, 585–607, <https://doi.org/10.5194/gmd-10-585-2017>, 2017.

- Dahlmann, K, Grewe, V., Ponater, M., Matthes, S., Quantifying the contributions of individual NO_x sources to the trend in ozone radiative forcing, *Atmos. Environ.* 45 (17), 2860-2868, DOI: 10.1016/j.atmosenv.2011.02.071, 2011
- 1305 Derwent, R. G., W. J. Collins, C. E. Johnson, D. S. Stevenson, Transient behaviour of tropospheric ozone precursors in a global 3-D CTM and their indirect greenhouse effects. *Climatic Change* 49, 463–487, <https://doi.org/10.1023/A:1010648913655>, 2001.
- 1310 Eastham, Sebastian D., and Steven R. H. Barrett. 2016. “Aviation-Attributable Ozone as a Driver for Changes in Mortality Related to Air Quality and Skin Cancer.” *Atmospheric Environment*. <https://doi.org/10.1016/j.atmosenv.2016.08.040>, 2016.
- Emanuel, K. A., A scheme for representing cumulus convection in large-scale models, *J Atmos. Sci.*, 48, 2313–2335, 1991.
- 1315 Etminan, M., G. Myhre, E. J. Highwood, K. P. Shine, Radiative forcing of carbon dioxide, methane, and nitrous oxide: A significant revision of the methane radiative forcing. *Geophysical Research Letters* 43,12,614–12,623 <https://doi.org/10.1002/2016GL071930>, 2016.
- Eyers, C.J., Addleton, D., Atkinson, K., Broomhead, M.J., Christou, R., Elliff, T., Falk, R., Gee, I., Lee, D.S., Marizy, C., Michot, S., Middel, J., Newton, P., Norman, P., Plohr, M., Raper, D., Stanciou, N., AERO2k Global Aviation Emissions Inventories for 2002 and 2025 QINETIQ/04/01113, Farnborough, Hants, UK., 2005.
- 1320 Federal Aviation Administration (FAA), Recommended best practice for quantifying speciated organic gas emissions from aircraft equipped with turbofan, turbojet and turboprop engines, 2009.
- Fiore, A. M., Dentener, F. J., Wild, O., Cuvelier, C., Schultz, M. G., Hess, P., et al. Multimodel estimates of intercontinental source - receptor relationships for ozone pollution. *Journal of Geophysical Research*, 114, D04301. <https://doi.org/10.1029/2008JD010816>, 2009.
- 1325 Folberth, G. A., D. A. Hauglustaine, P. Ciais, et J. Lathière, On the role of atmospheric chemistry in the global CO₂ budget, *Geophys. Res. Lett.* 32, L08801, doi:10.1029/2004GL021812, 2005.
- Folberth, G. A., D. A. Hauglustaine, J. Lathière, and F. Brocheton, Interactive chemistry in the Laboratoire de Météorologie Dynamique general circulation model: model description and impact analysis of biogenic hydrocarbons on tropospheric chemistry, *Atmos. Chem. Phys.*, 6, 2273–2319, 2006.
- 1330 Forster, P., T. Storelvmo, K. Armour, W. Collins, J.-L. Dufresne, D. Frame, D.J. Lunt, T. Mauritsen, M.D. Palmer, M. Watanabe, M. Wild, and H. Zhang, 2021: The Earth’s Energy Budget, Climate Feedbacks, and Climate Sensitivity. In *Climate Change 2021: The Physical Science Basis. Contribution of Working Group I to the Sixth Assessment Report of the Intergovernmental Panel on Climate Change* [Masson-Delmotte, V., P. Zhai, A. Pirani, S.L. Connors, C. Péan, S. Berger, N. Caud, Y. Chen, L. Goldfarb, M.I. Gomis, M. Huang, K. Leitzell, E. Lonnoy, J.B.R. Matthews, T.K. Maycock, T. Waterfield, O. Yelekçi, R. Yu, and B. Zhou (eds.)]. Cambridge University Press, Cambridge, United Kingdom and New York, NY, USA, pp. 923–1054, doi:10.1017/9781009157896.009, 2021.
- 1335 Fouquart, Y., and B. Bonel, Computations of solar heating of the earth's atmosphere: a new parameterization, *Beitr. Phys. Atmos.*, 53, 35-62, 1980.
- 1340 Freeman, S., D. S. Lee, L. L. Lim, A. Skowron, and R. Rodriguez De Leon, Trading off aircraft fuel burn and NO_x emissions for optimal climate policy. *Environ. Sci. Technol.* 52, 2498–2505, 2018.
- Frömming, C., Ponater, M., Dahlmann, K., Grewe, V., Lee, D.S., Sausen, R., Aviation-induced radiative forcing and surface temperature change in dependency of the emission altitude. *J. Geophys. Res.* 117 (D19), D19104, 2012.
- 1345 Fuglestad, J. S., T. K. Berntsen, I. S. A. Isaksen, H. T. Mao, X. Z. Liang, W. C. Wang, Climatic forcing of nitrogen oxides through changes in tropospheric ozone and methane; global 3D model studies. *Atmospheric Environment* 33, 961–977, 1999.
- 1350 Fuglestad, J. S., K. P. Shine, T. Berntsen, J. Cook, D. S. Lee, A. Stenke, R. B., Skeie, G. J. M. Velders, et I. A. Waitz, Transport impacts on atmosphere and climate: metrics, *Atmos. Environ.*, 44, 4648-4677, 2010.
- Gauss, M., Isaksen, I.S.A., Lee, D.S., Søvde, O.A., Impact of aircraft NO_x emissions on the atmosphere and tradeoffs to reduce the impact, *Atmos. Chem. Phys.* 6., 2006.
- 1355 Gidden, M. J., Riahi, K., Smith, S. J., Fujimori, S., Luderer, G., Kriegler, E., van Vuuren, D. P., van den Berg, M., Feng, L., Klein, D., Calvin, K., Doelman, J. C., Frank, S., Fricko, O., Harmsen, M., Hasegawa, T., Havlik, P., Hilaire, J., Hoesly, R., Horing, J., Popp, A., Stehfest, E., and Takahashi, K.: Global emissions pathways under different socioeconomic scenarios for use in CMIP6: a dataset of harmonized emissions trajectories through the end of the century, *Geosci. Model Dev.*, 12, 1443–1475, <https://doi.org/10.5194/gmd-12-1443-2019>, 2019.
- 1360 Gilmore, C. K., S. R H Barrett, J. Koo and Q. Wang, Temporal and spatial variability in the aviation NO_x-related O₃ impact, *Environ. Res. Lett.* 8 034027, 2013.
- Gliß, J., Mortier, A., Schulz, M., Andrews, E., Balkanski, Y., Bauer, S. E., Benedictow, A. M. K., Bian, H., Checa-Garcia, R., Chin, M., Ginoux, P., Griesfeller, J. J., Heckel, A., Kipling, Z., Kirkevåg, A., Kokkola, H., Laj, P., Le Sager, P., Lund, M. T., Lund Myhre, C., Matsui, H., Myhre, G., Neubauer, D., van Noije, T., North, P., Olivié, D. J. L., Rémy, S., Sogacheva, L., Takemura, T., Tsigaridis, K., and Tsyro, S. G.: AeroCom phase III multi-model evaluation of the aerosol life cycle and optical properties using ground- and space-based remote sensing as well as surface in situ observations, *Atmos. Chem. Phys.*, 21, 87–128, <https://doi.org/10.5194/acp-21-87-2021>, 2021.
- 1365

- Grewe, V., M. Dameris, C. Fichter, D. Lee, Impact of aircraft NO_x emissions. Part 2: Effects of lowering the flight altitude, *Meteorol. Z.* 3, 197-205, 2002.
- 1370 Grewe, V., and A. Stenke, AirClim: an efficient tool for climate evaluation of aircraft technology. *Atmospheric Chemistry and Physics* 8, 4621–4639, <https://doi.org/10.5194/acp-8-4621-2008>, 2008.
- Grewe, V., Frömming, C., Matthes, S., Brinkop, S., Ponater, M., Dietmüller, S., Jöckel, P., Garny, H., Tsati, E., Dahlmann, K., Søvde, O. A., Fuglestad, J., Berntsen, T. K., Shine, K. P., Irvine, E. A., Champougnny, T., and Hullah, P.: Aircraft routing with minimal climate impact: the REACT4C climate cost function modelling approach (V1.0), *Geosci. Model Dev.*, 7, 175-201, doi:10.5194/gmd-7-175-2014, 2014.
- 1375 Grewe V., Matthes S., Dahlmann K. The contribution of aviation NO_x to climate change: are we ignoring methodological flaws? *Environmental Research Letters* 14, 121003 (2019).
- Hanson, D., Ravishankara, A. R., and Solomon, S.: Heterogeneous reactions in sulfuric acid aerosols: A framework for model calculations, *J. Geophys. Res.*, 99, 36153629, 1988.
- 1380 Hauglustaine D. A., C. Granier, G. P. Brasseur et G. Mégie, Impact of present aircraft emissions of nitrogen oxides on tropospheric ozone and climate forcing, *Geophys. Res. Lett.*, 21, 2031-2034, 1994.
- Hauglustaine, D. A., Hourdin, F., Jourdain, L., Filiberti, M. A., Walters, S., Lamarque, J. F., and Holland, E. A.: Interactive chemistry in the Laboratoire de Meteorologie Dynamique general circulation model: Description and background tropospheric chemistry evaluation, *J. Geophys. Res.*, 109, D04314, doi:10.1029/2003JD003957, 2004.
- 1385 Hauglustaine, D.A. and B. Koffi, Boundary layer ozone pollution caused by future aircraft emissions, *Geophys. Res. Lett.*, 39, L13808, 2012.
- Hauglustaine, D. A., Balkanski, Y., and Schulz, M.: A global model simulation of present and future nitrate aerosols and their direct radiative forcing of climate, *Atmos. Chem. Phys.*, 14, 11031-11063, doi:10.5194/acp-14-11031-2014, 2014.
- 1390 Hodnebrog, Ø., Berntsen, T. K., Dessens, O., Gauss, M., Grewe, V., Isaksen, I. S. A., Koffi, B., Myhre, G., Olivie, D., Prather, M. J., Pyle, J. A., Stordal, F., Szopa, S., Tang, Q., van Velthoven, P., Williams, J. E., and Ødemark, K.: Future impact of non-land based traffic emissions on atmospheric ozone and OH – an optimistic scenario and a possible mitigation strategy, *Atmos. Chem. Phys.*, 11, 11293-11317, doi:10.5194/acp-11-11293-2011, 2011.
- 1395 Hodnebrog, Ø., T. K. Berntsen, O. Dessens, M. Gauss, V. Grewe, I. S. A. Isaksen, B. Koffi, G. Myhre, D. Olivie, M. J. Prather, F. Stordal, S. Szopa, Q. Tang, P. van Velthoven, J. E. Williams, Future impact of traffic emissions on atmospheric ozone and OH based on two scenarios. *Atmospheric Chemistry and Physics* 12, 12,211–12,225, <https://doi.org/10.5194/acp-12-12211-2012>, 2012.
- 1400 Hoesly, R. M., Smith, S. J., Feng, L., Klimont, Z., Janssens-Maenhout, G., Pitkanen, T., Seibert, J. J., Vu, L., Andres, R. J., Bolt, R. M., Bond, T. C., Dawidowski, L., Kholod, N., Kurokawa, J.-I., Li, M., Liu, L., Lu, Z., Moura, M. C. P., O'Rourke, P. R., and Zhang, Q.: Historical (1750–2014) anthropogenic emissions of reactive gases and aerosols from the Community Emissions Data System (CEDS), *Geosci. Model Dev.*, 11, 369–408, <https://doi.org/10.5194/gmd-11-369-2018>, 2018.
- 1405 Holmes, C. D., Methane feedback on atmospheric chemistry: Methods, models, and mechanisms. *Journal of Advances in Modeling Earth Systems*, 10, 1087–1099. <https://doi.org/10.1002/2017MS001196>, 2018.
- Holmes, C. D., Q. Tang, et M. Prather, Uncertainties in climate assessment for the case of aviation NO_x, *Proceedings of the National Academy of Sci.*, 108, 10997-11002, 2011.
- 1410 Hoor, P., Borken-Kleefeld, J., Caro, D., Dessens, O., Endresen, O., Gauss, M., Grewe, V., Hauglustaine, D., Isaksen, I. S. A., Jöckel, P., Lelieveld, J., Myhre, G., Meijer, E., Olivie, D., Prather, M., Schnadt Poberaj, C., Shine, K. P., Staehelin, J., Tang, Q., van Aardenne, J., van Velthoven, P., and Sausen, R.: The impact of traffic emissions on atmospheric ozone and OH: results from QUANTIFY, *Atmos. Chem. Phys.*, 9, 3113–3136, doi:10.5194/acp-9-3113-2009, 2009.
- Hourdin, F. and A. Armengaud, The use of finite-volume methods for atmospheric advection of trace species I. Test of various formulations in a general circulation model, *Month. Weather Rev.*, 127, 822-837, 1999
- Hourdin, F. and J. P. Issartel, Sub-surface nuclear tests monitoring through the CTBT xenon network, *Geophys. Res. Lett.*, 27, 2245-2248, 2000.
- Hourdin, F., C. R., Grandpeix, J.-Y., Madeleine, J.-B., Chérut, F., Rochetin, N., Musat, I., Idelkadi, A., Fairhead, L., Foujols, M.-A., Mellul, L., Traore, A.-K., Dufresne, J.-L., Boucher, O., Lefebvre, M.-P., Millour, E., Vignon, E., Jouaud, J., Diallo, F. B., Lott, F., Caubel, A., Meurdesoif, Y., and Ghattas, J.: LMDZ6A: the atmospheric component of the IPSL climate model with improved and better tuned physics, *J. Adv. Model. Earth Syst.*, <https://doi.org/10.1029/2019MS001892>, 2020.
- 1420 Huszar, P., Teyssède, H., Michou, M., Voldoire, A., Olivie, D. J. L., Saint-Martin, D., Cariolle, D., Senesi, S., Salas Y Melia, D., Alias, A., Karcher, F., Ricaud, P., and Halenka, T.: Modeling the present and future impact of aviation on climate: an AOGCM approach with online coupled chemistry, *Atmos. Chem. Phys.*, 13, 10027–10048, <https://doi.org/10.5194/acp-13-10027-2013>, 2013.
- 1425 Ivanovich, C. C., Ocko, I. B., Piris-Cabezas, P., and Petsonk, A.: Climate benefits of proposed carbon dioxide mitigation strategies for international shipping and aviation, *Atmos. Chem. Phys.*, 19, 14949–14965, <https://doi.org/10.5194/acp-19-14949-2019>, 2019.
- 1430 Jourdain, L. et D. A. Hauglustaine, The global distribution of lightning NO_x simulated on-line in a general circulation model, *Phys. Chem. Earth*, 26, 585-591, 2001.
- Kapadia, Z. A., et al., Impacts of aviation fuel sulfur content on climate and human health, *Atmos. Chem. Phys.*, 16, 10521-10541, 2016.

- 1435 Kärcher, B. Formation and radiative forcing of contrail cirrus. *Nature Communications* 9:1824, <https://doi.org/10.1038/s41467-018-04068-0>, 2018.
- Khodayari, A., S. Tilmes, S. C. Olsen, D. B. Phoenix, D. J. Wuebbles, J.-F. Lamarque, C.-C. Chen, Aviation 2006 NO_x-induced effects on atmospheric ozone and HO_x in Community Earth System Model (CESM). *Atmospheric Chemistry and Physics* 14, 9925–9939, <https://doi.org/10.5194/acp-14-9925-2014>, 2014a.
- 1440 Khodayari, A., S. C. Olsen, D. J. Wuebbles, Evaluation of aviation NO_x-induced radiative forcings for 2005 and 2050. *Atmospheric Environment* 91, 95–103, <https://doi.org/10.1016/j.atmosenv.2014.03.044>, 2014b.
- Khodayari, A., S. C. Olsen, D. J. Wuebbles, and D. B. Phoenix, Aviation NO_x-induced CH₄ effect: fixed mixing ratio boundary conditions versus flux boundary conditions, *Atmos. Environ.*, 113, 135–139, 2015.
- Kinnison, D. E. et al. Sensitivity of chemical tracers to meteorological parameters in the MOZART-3 chemical transport model. *J. Geophys. Res.* 112, D20302, 2007.
- 1445 Koffi, B., S. Szopa, A. Cozic, D. Hauglustaine and P. VanVelthoven, Present and future impact of aircraft, road traffic and shipping emissions on global tropospheric ozone, *Atmos. Chem. Phys.*, 10, 11681–11705, 2010.
- Koffi, B., M. Schulz, F.-M. Bréon, F. Dentener, B. M. Steensen, J. Griesfeller, D. Winker, Y. Balkanski, S. Bauer, N. Bellouin, T. Berntsen, H. Bian, M. Chin, T. Diehl, R. Easter, S. Ghan, D. A. Hauglustaine, T. Iversen, A. Kirkevåg, X. Liu, U. Lohmann, G. Myhre, P. Rasch, O. Seland, R. B. Skeie, S. D. Steenrod, P. Stier, T. Takemura, K. Tsigaridis, M. R. Vuolo, J. Yoon, K. Zhang, Evaluation of the aerosol vertical distribution in global transport models through comparison against CALIOP measurements: update based on the AeroCom phase II simulations, *J. Geophys. Res.*, 121, 7254–7283, doi:10.1002/2015JD024639, 2016.
- 1450 Krinner, G., N. Viovy, N. de Noblet-Ducoudre, J. Ogee, J. Polcher, P. Friedlingstein, P. Ciais, S. Sitch, and I. C. Prentice, A dynamic global vegetation model for studies of the coupled atmosphere- biosphere system, *Global Biogeochem. Cycles*, 19, GB1015, doi: 10.1029/2003GB002199, 2005.
- 1455 Lamarque J.-F., T. C. Bond, V. Eyring, C. Granier, A. Heil, Z. Klimont, D. Lee, C. Liousse, A. Mieville, B. Owen, M. G. Schultz, D. Shindell, S. J. Smith, E. Stehfest, J. Van Aardenne, O. R. Cooper, M. Kainuma, N. Mahowald, J. R. McConnell, V. Naik, K. Riahi, and D. P. van Vuuren, Historical (1850–2000) gridded anthropogenic and biomass burning emissions of reactive gases and aerosols: methodology and application, *Atmos. Chem. Phys.*, 10, 7017–7039, 2010.
- 1460 Lamarque, J.-F., G. P. Kyle, M. Meinshausen, K. Riahi, S. J. Smith, D. P. van Vuuren, A. J. Conley, and F. Vitt, Global and regional evolution of short-lived radiatively-active gases and aerosols in the Representative Concentration Pathways, *Climatic Change*, 109:191–212 doi :10.1007/s10584-011-0155-0, 2011.
- 1465 Lathièrè, J., D. A. Hauglustaine, N. De Noblet-Ducoudré, G. Krinner, et G. A. Folberth, Past and future changes in biogenic volatile organic compound emissions simulated with a global dynamic vegetation model, *Geophys. Res. Lett.*, 32, L20818, doi:10.1029/2005GL024164, 2005.
- Lee D. S., Fahey, D. W., Forster, P. M., et al.: Aviation and global climate change in the 21st century, *Atmos. Environ.*, 43, 3520–3537, 2009.
- 1470 Lee, D. S., Pitari, G., Grewe, V., Gierens, K., Penner, J. E., Pet- zold, A., Prather, M. J., Schumann, U., Bais, A., Berntsen, T., Iachetti, D., Lim, L. L., and Sausen, R.: Transport impacts on atmosphere and climate: Aviation, *Atmos. Environ.*, 44, 4678–4734, doi:10.1016/j.atmosenv.2009.06.005, 2010.
- Lee, D. S., Fahey, D. W., Skowron, A., Allen, M. R., Burkhardt, U., Chen, Q., Doherty, S. J., Freeman, S., Forster, P. M., Fuglestedt, J., Gettelman, A., De Léon, R. R., Lim, L. L., Lund, M. T., Millar, R. J., Owen, B., Penner, J. E., Pitari, G., Prather, M. J., Sausen, R., Wilcox, L. J. The contribution of global aviation to anthropogenic climate forcing for 2000 to 2018. *Atmos. Environ.*, 244, 117834, 2021.
- 1475 Lee, H., Olsen, S.C., Wuebbles, D.J., Youn, D., Impacts of aircraft emissions on the air quality near the ground. *Atmos. Chem. Phys.* 13, 5505–5522. doi:10.5194/acp-13-5505-2013, 2013.
- Lefèvre, F., G. P. Brasseur, I. Folkins, A. K. Smith, and P. Simon, Chemistry of the 1991-1992 stratospheric winter: threedimensional model simulations, *J. Geophys. Res.*, 99, 8183, 1994.
- 1480 Li B., T. Gasser, P. Ciais, S. Piao, S. Tao, Y. Balkanski, D. Hauglustaine, J.-P. Boisier, Z. Chen, L. Z. Li, Y. Li, H. Liu, J. Liu, S. Peng, Z. Sun, R. Wang, T. Wang, G. Yin, Y. Yin, Z. Zeng, and F. Zhou, The contribution of China’s emissions to global climate forcing, *Nature*, 531, 357–362, 2016.
- Lim, L. L., D. S. Lee, B. Owen, A. Skowron, S. Matthes, U. Burkhardt, S. Dietmuller, G. Pitari, G. Di Genova, D. Iachetti, I. Isaksen, O. A. Søvde, REACT4C: Simplified mitigation study. TAC-4 Proceedings, June 22nd to 25th, 2015, Bad Kohlgrub, 181–185, 2015.
- 1485 Lund, M. T., Aamaas, B., Berntsen, T., Bock, L., Burkhardt, U., Fuglestedt, J. S., and Shine, K. P.: Emission metrics for quantifying regional climate impacts of aviation, *Earth Syst. Dynam.*, 8, 547–563, <https://doi.org/10.5194/esd-8-547-2017>, 2017.
- 1490 Marengo, A., Thouret, V., Nédélec, P., Smit, H., Helten, M., Kley, D., Karsher, F., Simon, P., Law, K., Pyle, J., Poschmann, G., Von Wrede, R., Hume, C., and Cook, T.: Measurement of ozone and water vapour by Airbus in-service aircraft: The MOZAIC airborne programme, an overview, *J. Geophys. Res.*, 103, 25 631–25 642, doi:10.1029/98JD00977, 1998.
- Matthes, S., Schumann, U., Grewe, V., Frömming, C., Dahlmann, K., Koch, A., and Mannstein, H.: Climate Optimized Air Transport, edited by: Schumann, U., ISBN 978-3-642-30182-7, ISBN 978-3-642-30183-4 (eBook), doi:10.1007/978-3-642-30183-4, Springer, Heidelberg, New York, 2012.
- 1495 Matthes, S., Grewe, V., Dahlmann, K., Frömming, C., Irvine, E., Lim, L., Linke, F., Lührs, B., Owen, B., Shine, K., Stromatas, S., Yamashita, H., Yin, F., A concept for multi-dimensional environmental assessment of aircraft trajectories, *Aerospace* 4(3), 42; doi:10.3390/aerospace4030042, 2017.

- 1500 Matthes., S, Lim, L., Burkhardt, U., Dahlmann, K., Dietmüller, S., Grewe, V. Haslerud, A.S., Hendricks, J., Owen, B., Pitari, G., Righi, M., Skowron, A. Mitigation of non-CO₂ aviation's climate impact by changing cruise altitudes. *Aerospace*, 8(2), 36., 2021
- Morcrette, J.-J., Radiation and cloud radiative properties in the European Centre for Medium Range Weather Forecasts forecasting system, *J. Geophys. Res.*, 96, 9121-9132, 1991.
- 1505 Morris, G.A., Rosenfield, J.E., Schoeberl, M.R., Jackman, C.H., Potential impact of subsonic and supersonic aircraft exhaust on water vapour in the lower stratosphere assessed via a trajectory model. *Journal of Geophysical Research*, 108, 4103, 2003.
- Myhre, G., M. Kvalevåg, G. Rädcl, J. Cook, K. P. Shine, H. Clark, F. Karcher, K. Markowicz, A. Kardas, P. Wolkenberg, Y. Balkanski, M. Ponater, P. Forster, A. Rap, R. R. de Leon, Intercomparison of radiative forcing calculations of stratospheric water vapour and contrails. *Meteorologische Zeitschrift* 18, 585–596, <https://doi.org/10.1127/0941-2948/2009/0411>, 2009.
- 1510 Myhre, G., K. P. Shine, G. Rädcl, M. Gauss, I. S. A. Isaksen, Q. Tang, M. J. Prather, J. E. Williams, P. van Velthoven, O. Dessens, B. Koffi, S. Szopa, P. Hoor, V. Grewe, J. Borcken-Kleefeld, T. K. Berntsen, J. S. Fuglestedt, Radiative forcing due to changes in ozone and methane caused by the transport sector. *Atmospheric Environment* 45, 387–394, <https://doi.org/10.1016/j.atmosenv.2010.10.001>, 2011.
- 1515 Myhre, G., and 40 co-authors, Radiative forcing of the direct aerosol effect from AEROCOM Phase II simulations, *Atmos. Chem. Phys.*, 13, 1853-1877, 2013.
- Naik, V., S. Szopa, B. Adhikary, P. Artaxo, T. Berntsen, W. D. Collins, S. Fuzzi, L. Gallardo, A. Kiendler Scharr, Z. Klimont, H. Liao, N. Unger, P. Zanis, Short-Lived Climate Forcers. In: *Climate Change 2021: The Physical Science Basis. Contribution of Working Group I to the Sixth Assessment Report of the Intergovernmental Panel on Climate Change* [Masson-Delmotte, V., P. Zhai, A. Pirani, S. L. Connors, C. Péan, S. Berger, N. Caud, Y. Chen, L. Goldfarb, M. I. Gomis, M. Huang, K. Leitzell, E. Lonnoy, J. B. R. Matthews, T. K. Maycock, T. Waterfield, O. Yelekçi, R. Yu and B. Zhou (eds.)], Cambridge University Press. 2022.
- 1520 Nakicenovic, N., and R. Swart (eds), IPCC special report on emissions scenarios, Cambridge University Press, Cambridge, 2000.
- 1525 Nédélec, P., Cammas, J.-P., Thouret, V., Athier, G., Cousin, J.-M., Legrand, C., Abonnel, C., Lecoœur, F., Cayez, G., and Marizy, C.: An improved infrared carbon monoxide analyser for routine measurements aboard commercial Airbus aircraft: technical validation and first scientific results of the MOZAIC III programme, *Atmos. Chem. Phys.*, 3, 1551–1564, doi:10.5194/acp-3-1551-2003, 2003.
- 1530 Nédélec, P., Blot, R., Boulanger, D., Athier, G., Cousin, J.-M., Gautron, B., Petzold, A., Volz-Thomas, A., and Thouret, V.: Instrumentation on commercial aircraft for monitoring the atmospheric composition on a global scale: the IAGOS system, technical overview of ozone and carbon monoxide measurements, *Tellus B*, 67, 27–791, doi:10.3402/tellusb.v67.27791, 2015.
- Olsen, S.C., G.P. Brasseur, D.J. Wuebbles, S.R.H. Barrett, H. Dang, S.D. Eastham, M.Z. Jacobson, A. Khodayari, H. Selkirk, A. Sokolov, N. Unger et al., Comparison of model estimates of the effects of aviation emissions on atmospheric ozone and methane, *Geophys. Res. Lett.*, 40, 6004–6009, 2013.
- 1535 Olivié, D. J. L., Cariolle, D., Teyssède, H., Salas, D., Voldoire, A., Clark, H., Saint-Martin, D., Michou, M., Karcher, F., Balkanski, Y., Gauss, M., Dessens, O., Koffi, B., and Sausen, R.: Modeling the climate impact of road transport, maritime shipping and aviation over the period 1860–2100 with an AOGCM, *Atmos. Chem. Phys.*, 12, 1449–1480, <https://doi.org/10.5194/acp-12-1449-2012>, 2012.
- 1540 Owen, B., Lee, D. S., and Lim, L., Flying into the future: aviation emissions scenarios to 2050, *Environmental Science and Technology*, 44(7), 2255-2260, doi: 10.1021/es902530z, 2010.
- Penner, J.E., D.H. Lister, D.J. Griggs, D.J. Dokken, and M. McFarland (Eds.), Aviation and the global atmosphere, Intergovernmental Panel on Climate Change (IPCC), Cambridge University Press, 1999.
- 1545 Petzold, A., Thouret, V., Gerbig, C., Zahn, A., Brenninkmeijer, C., Gallagher, M., Hermann, M., Pontaud, M., Ziereis, H., Boulanger, D., Marshall, J., Nédélec, P., Smit, H., Friess, U., Flaud, J.-M., Wahner, A., Cammas, J.-P., and Volz-Thomas, A.: Global-scale atmosphere monitoring by in-service aircraft - current achievements and future prospects of the European Research Infrastructure IAGOS, *Tellus B*, 67, doi:10.3402/tellusb.v67.28452, 2015.
- 1550 Pitari G., D. Iachetti, G. Di Genova, N. De Luca, O.A. Søvdø, Ø. Hodnebrog, D.S. Lee, L. Lim, Impact of coupled NO_x/aerosol aircraft emissions on ozone photochemistry and radiative forcing. *Atmosphere*, 6, 751–782; 2015.
- Pitari, G., E. Mancini, and A. Bregman, Climate forcing of subsonic aviation: Indirect role of sulfate particles via heterogeneous chemistry, *Geophys. Res. Lett.*, 29(22), 2057, doi:10.1029/2002GL015705, 2002.
- 1555 Pitari, G., I. Cionni, G. Di Genova, O. Søvdø, and Ling Lim, Radiative forcing from aircraft emissions of NO_x : model calculations with CH₄ surface flux boundary condition, *Meteorol. Zeitschrift*, 2016.
- Prashanth, P., R. L. Speth, S. D. Eastham, J. S. Sabnis, and S.R.H. Barrett, Post-Combustion Emissions Control in Aero-Gas Turbine Engines. *Energy and Environmental Science*, DOI: 10.1039/D0EE02362K, 2021.
- Prashanth, P., S. D. Eastham, R. L. Speth, and S.R.H. Barrett, Aerosol formation pathways from aviation emissions. *Energy and Environmental Science*, DOI: 10.1039/D0EE02362K, 2022.
- 1560 Prather, M. J., Lifetimes and eigenstates in atmospheric chemistry. *Geophysical Research Letters* 21, 801–804, <https://doi.org/10.1029/94GL00840>, 1994.
- Prather, M., D. Ehhalt, F. Dentener, R. Derwent, E. Dlugokencky E, “Atmospheric chemistry and greenhouse gases”, in *Climate Change 2001: The Scientific Basis, Contribution of Working Group I to the Third*

- 1565 Assessment Report of the Intergovernmental Panel on Climate Change, J. T. Houghton ed. (Cambridge University Press, Cambridge, United Kingdom and New York, NY, USA, 2001) pp. 239–287, 2001.
- Righi, M., Hendricks, J., and Sausen, R.: The global impact of the transport sectors on atmospheric aerosol: simulations for year 2000 emissions, *Atmos. Chem. Phys.*, 13, 9939–9970, doi:10.5194/acp-13-9939-2013, 2013.
- 1570 Righi, M., Hendricks, J., & Sausen, R. (2016). The global impact of the transport sectors on atmospheric aerosol in 2030; Part 2 : Aviation. *Atmos. Chem. Phys.*, 16(7), 4481–4495. <https://doi.org/10.5194/acp-16-4481-2016>.
- Schulz, M., Constraining Model Estimates of the Aerosol Radiative Forcing, Thèse d’Habilitation à Diriger des Recherches, Université Pierre et Marie Curie, Paris VI, 2007.
- 1575 Schulz, M., Y. Balkanski, F. Dulac, and W. Guelle, Role of aerosol size distribution and source location in a three-dimensional simulation of a Saharan dust episode tested against satellite-derived optical thickness, *J. Geophys. Res.*, 103, 10,579–10,592, 1998.
- Skowron, A., D. S. Lee, R. R., De Leon, The assessment of the impact of aviation NO_x on ozone and other radiative forcing responses – The importance of representing cruise altitude accurately, *Atmos. Environ.*, 74, 159–168, 2013.
- 1580 Skowron, A., D. S. Lee, R. R. De León, L. L. Lim, B. Owen, Greater fuel efficiency is potentially preferable to reducing NO_x emissions for aviation’s climate impacts. *Nature Communications*. 12, 2021.
- Søvde, O. A., Gauss, M., Isaksen, I. S. A., Pitari, G., and Marizy, C.: Aircraft pollution – a futuristic view, *Atmos. Chem. Phys.*, 7, 3621–3632, <https://doi.org/10.5194/acp-7-3621-2007>, 2007.
- 1585 Søvde, O.A., S. Matthes, A. Skowron, D. Iachetti, L. Lim, L., Ø. Hodnebrog, G. Di Genova, G. Pitari, D.S. Lee, G. Myhre, I.S.A. Isaksen, Aircraft emission mitigation by changing route altitude: A multi-model estimate of aircraft NO_x emission impact on O₃ photochemistry, *Atmospheric Environment*, 95, 468–479, 2014.
- Stevenson, D. S., R. M. Doherty, M. G. Sanderson, W. J. Collins, C. E. Johnson, R. G. Derwent, Radiative forcing from aircraft NO_x emissions: mechanisms and seasonal dependence *Journal of Geophysical Research Atmospheres* 109, D17307, <https://doi.org/10.1029/2004JD004759>, 2004.
- 1590 Stevenson, D.S. and R.G. Derwent: How does the location of aircraft nitrogen oxide emissions affect their climate impact? *Geophys. Res. Lett.*, 36, L17810, doi:10.1029/2009GL039422, 2009.
- Terrenoire, E., D. A. Hauglustaine, T. Gasser and O. Penanhoat, The contribution of carbon dioxide emissions from the aviation sector to future climate change, *Environ. Res. Lett.* 14 084019, 2019.
- 1595 Thomason, L. W., Ernest, N., Millán, L., Rieger, L., Bourassa, A., Vernier, J.-P., Manney, G., Luo, B., Arfeuille, F., and Peter, T.: A global space-based stratospheric aerosol climatology: 1979–2016, *Earth Syst. Sci. Data*, 10, 469–492, <https://doi.org/10.5194/essd-10-469-2018>, 2018.
- Thouret, V., Marenco, A., Logan, J. A., Nédélec, P., and Grouhel, C.: Comparisons of ozone measurements from the MOZAIC airborne program and the ozone sounding network at eight locations, *J. Geophys. Res.*, 103, 25 695–25 720, doi:10.1029/98JD02243, 1998.
- 1600 Tilmes, S., J.-F. Lamarque, L. K. Emmons, A. Conley, M. G. Schultz, M. Saunio, V. Thouret, A. M. Thompson, S. J. Oltmans, B. Johnson, and D. Tarasick. Technical Note: Ozonesonde climatology between 1995 and 2011: description, evaluation and applications. *Atmos. Chem. Phys.*, 12, 7475–7497, 2012.
- Unger, N.: Global climate impact of civil aviation for standard and desulfurized jet fuel, *Geophys. Res. Lett.*, 38, 1–6, doi:10.1029/2011GL049289, 2011.
- 1605 Unger, N., Zhao, Y., and Dang, H.: Mid-21st century chemical forcing of climate by the civil aviation sector, *Geophys. Res. Lett.*, 40, 641–645, doi:10.1002/grl.50161, 2013.
- Van Leer, B., Towards the ultimate conservative difference scheme. Part IV: a new approach to numerical convection, *J. Comput. Phys.*, 23, 276–299, 1977.
- 1610 Voulgarakis, A., V. Naik, J.-F. Lamarque, D. T. Shindell, P. J. Young, M. J. Prather, O. Wild, R. D. Field, 1259 D. Bergmann, P. Cameron-Smith, I. Cionni, W. J. Collins, S. B. Dalsøren, R. M. Doherty, V. Eyring, G. 1260 Faluvegi, G. A. Folberth, L. W. Horowitz, B. Josse, I. A. McKenzie, T. Nagashima, D. A. Plummer, M. Righi, S. T. Rumbold, D. S. Stevenson, S. A. Strode, K. Sudo, S. Szopa, G. Zeng, Analysis of present-day 1262 and future OH and methane lifetime in the ACCMIP simulations. *Atmospheric Chemistry and Physics* 13, 2563–2587, <https://doi.org/10.5194/acp-13-2563-2013>, 2013.
- 1615 Wilcox, L., K. P. Shine, B. J. Hoskins, Radiative forcing due to aviation water vapour emissions. *Atmospheric Environment* 63, 1–13, <https://doi.org/10.1016/j.atmosenv.2012.08.072>, 2012.
- Wilkerson, J. T., Jacobson, M. Z., Malwitz, A., Balasubramanian, S., Wayson, R., Fleming, G., Naiman, A. D., and Lele, S. K.: Analysis of emission data from global commercial aviation: 2004 and 2006, *Atmos. Chem. Phys.*, 10, 6391–6408, <https://doi.org/10.5194/acp-10-6391-2010>, 2010.
- 1620 Yim, S. H. L., G. L. Lee, I. H. Lee, F. Allroggen, A. Ashok, F. Caiazzo, S. D. Eastham, R. Malina and S. R. H. Barrett, Global, regional and local health impacts of civil aviation emissions, *Environ. Res. Lett.*, 1, 034001, 2015.

1625

1630

Table 1. Total global aircraft emissions corresponding to the baseline REACT4C_2006 and QUANTIFY_2000 inventories.

Species	Units	REACT4C_2006	QUANTIFY_2000
Fuel	Tg yr ⁻¹	178	214
CO ₂	Tg yr ⁻¹	560	672
NO _x	TgN yr ⁻¹	0.71	0.84
BC	Gg yr ⁻¹	4.0	5.0
SO ₂	GgS yr ⁻¹	71	85
HC	Gg yr ⁻¹	63	91
OC	Gg yr ⁻¹	8.8	10.0
SO ₄	GgS yr ⁻¹	2.3	2.8
H ₂ O	Tg yr ⁻¹	220	264
CO	Tg yr ⁻¹	0.51	0.72

1635

Table 2. Total global aircraft emissions for future 2050 baseline scenario QUANTIFY_A1 and for the two mitigation scenarios QUANTIFY_B1 and QUANTIFY_B1 ACARE.

Species	Units	A1	B1	B1 ACARE
Fuel	Tg yr ⁻¹	716	434	313
CO ₂	Tg yr ⁻¹	2257	1367	986
NO _x	TgN yr ⁻¹	3.3	1.0	0.69
BC	Gg yr ⁻¹	16.0	8.9	6.4
SO ₂	GgS yr ⁻¹	280	170	120
HC	Gg yr ⁻¹	280	150	110
OC	Gg yr ⁻¹	35.0	21.0	15.0
SO ₄	GgS yr ⁻¹	9.3	5.5	4.1
H ₂ O	Tg yr ⁻¹	886	537	387
CO	Tg yr ⁻¹	2.3	1.3	0.93

1645

Table 3. LMDZ-INCA model simulations performed in this study.

Simulation	Description
	« Present-day »
Base case	No aircraft emissions.
REACT4C_2006	« Present-day » with REACT4C_2006 aircraft emissions.
REACT4C_PLUS	REACT4C_2006 with aircraft flight altitude increased by 2000 ft.
REACT4C_MINUS	REACT4C_2006 with aircraft flight altitude decreased by 2000 ft.
QUANTIFY_2000	« Present-day » with QUANTIFY_2000 aircraft emissions.
	Future (2050)
Base case	No aircraft emissions.
QUANTIFY_A1	Reference future with QUANTIFY_A1 aircraft emissions.
QUANTIFY_A1_LowNOx	Future with QUANTIFY_A1 aircraft emissions with NO _x emissions/2.
QUANTIFY_A1_Desulfurized	Future with QUANTIFY_A1 aircraft emissions with SO _x emissions=0.
QUANTIFY_B1	Future with QUANTIFY_B1 aircraft mitigation emissions.
QUANTIFY_B1 ACARE	Future with QUANTIFY_B1 ACARE aircraft mitigation emissions.

1650

1655

Table 4. Annual aircraft NO_x emissions (ENO_x, TgN), ozone burden variation (ΔO_3 , TgO₃), ozone to NO_x sensitivity ($\Delta O_3/ENO_x$, TgO₃/TgN), methane lifetime variation ($\Delta\tau_{CH_4}$, %) and methane lifetime to NO_x sensitivity ($\Delta\tau_{CH_4}/ENO_x$, %/TgN), for the various simulations.

1660

Scenario	ENO _x	ΔO_3	$\Delta O_3/ENO_x$	$\Delta\tau_{CH_4}$	$\Delta\tau_{CH_4}/ENO_x$
REACT4C_2006	0.71	4.67	6.58	-1.01	-1.43
QUANTIFY_2000	0.84	5.05	6.01	-1.15	-1.37
REACT4C_PLUS	0.72	5.35	7.47	-1.02	-1.41
REACT4C_MINUS	0.71	4.15	5.84	-1.01	-1.42
QUANTIFY_A1	3.31	20.33	6.14	-4.67	-1.41
QUANTIFY_A1_LowNOx	1.66	11.34	6.83	-2.62	-1.58
QUANTIFY_A1_Desulfurized	3.31	20.18	6.09	-4.66	-1.41
QUANTIFY_B1	1.04	7.95	7.67	-1.76	-1.69
QUANTIFY_B1 ACARE	0.69	5.46	7.91	-1.19	-1.73

1665

Table 5. Radiative forcings of ozone, methane, black carbon (BC), sulfates, nitrates, organic carbon (OC) and stratospheric water vapour calculated for the different simulations (mW/m²). The radiative forcing of methane is the sum of 4 terms as depicted in **Table 5**.

1670

Scenario	F _{O3}	F _{CH4}	F _{BC}	F _{SO4}	F _{NO3}	F _{OC}	F _{H2O}	Total
REACT4C_2006	15.87	-14.69	0.46	-3.87	0.07	-0.03	0.13	-2.06
REACT4C_2006_NOx_Only	15.90	-14.72	0.00	-2.00	-0.12	0.00	0.00	-0.93
QUANTIFY_2000	17.19	-16.69	0.54	-4.33	0.06	-0.04	0.16	-3.12
REACT4C_PLUS	17.72	-14.80	0.49	-4.38	0.12	-0.04	0.17	-0.72
REACT4C_MINUS	14.28	-14.68	0.44	-3.40	0.03	-0.03	0.10	-3.24
QUANTIFY_A1	70.56	-70.84	1.88	-13.66	1.29	-0.16	0.52	-10.40
QUANTIFY_A1_LowNOx	39.29	-39.45	1.86	-10.88	1.69	-0.15	0.52	-7.11
QUANTIFY_A1_Desulfurized	70.08	-70.65	1.89	-6.47	-0.84	-0.16	0.52	-5.63
QUANTIFY_B1	27.57	-26.43	1.12	-7.38	1.17	-0.10	0.32	-3.73
QUANTIFY_B1 ACARE	18.74	-17.90	0.84	-5.20	0.85	-0.07	0.23	-2.52

1675

1680

Table 6. Decomposition of the total methane forcing F_{CH_4} into its various direct and indirect forcings. The forcings are associated with changes in methane lifetime (CH₄-OH), tropospheric ozone production (CH₄-O₃), stratospheric water vapour production (CH₄-SWV) and CO₂ production (CH₄-CO₂) (mW/m²).

Scenario	$F_{\text{CH}_4\text{-OH}}$	$F_{\text{CH}_4\text{-O}_3}$	$F_{\text{CH}_4\text{-SWV}}$	$F_{\text{CH}_4\text{-CO}_2}$	F_{CH_4}
REACT4C_2006	-11.02	-2.82	-0.65	-0.20	-14.69
REACT4C_2006_NOx_Only	-11.04	-2.83	-0.65	-0.20	-14.72
QUANTIFY_2000	-12.52	-3.20	-0.74	-0.23	-16.69
QUANTIFY_A1	-52.85	-13.96	-3.22	-0.81	-70.84
QUANTIFY_A1_LowNOx	-29.37	-7.8	-1.80	-0.45	-39.45
QUANTIFY_A1_Desulfurized	-52.71	-13.93	-3.21	-0.80	-70.65
QUANTIFY_B1	-19.66	-5.25	-1.21	-0.30	-26.43
QUANTIFY_B1_ACARE	-13.31	-3.56	-0.82	-0.21	-17.90

1685

1690

Table 7. Comparison of ozone, methane, black carbon (BC), sulfates, nitrates, organic carbon (OC) and stratospheric water vapour Radiative Forcings (RFs) and Effective Radiative Forcings (ERFs) calculated for the REACT4C_2006 simulation and compared to Lee et al. (2021) (mW/m²). For this comparison the REACT4C_2006 forcings are rescaled based on the total aviation fuel for 2018 and the ERF/RF factors provided by Lee et al. (2021) are applied to derive the ERFs. For methane, the correction factor (0.79) recalculated by Lee et al. (2021) for the year 2018 to account for the non-steady-state CH₄ responses to NO_x emission are also applied. The RFs and ERFs from Lee et al. (2021) provide the median and 5-95% confidence intervals, and the total forcings were recalculated based on a 10⁶ Monte-Carlo sampling from the discrete pdf provided by Lee et al. (2021).

1695

1700

	Lee et al. (2021)		This work	
	RF	ERF	RF	ERF
F_{O_3}	36.0 ⁵⁶ ₂₃	49.3 ⁷⁶ ₃₂	29.3	40.1
F_{CH_4}	-29.6 ⁻²¹ ₋₅₅	-34.9 ⁻²⁵ ₋₆₅	-21.4	-25.3
F_{BC}	0.94 ^{4.0} _{0.1}	0.94 ^{4.0} _{0.1}	0.86	0.86
F_{SO_4}	-7.4 ^{-2.6} ₋₁₉	-7.4 ^{-2.6} ₋₁₉	-7.1	-7.1
F_{NO_3}	–	–	0.14	0.14
F_{OC}	–	–	-0.06	-0.06
$F_{\text{H}_2\text{O}}$	2.0 ^{3.2} _{0.8}	2.0 ^{3.2} _{0.8}	0.24	0.24
Total	0.8²⁴₋₂₈	8.6³⁸₋₂₆	2.0	8.9

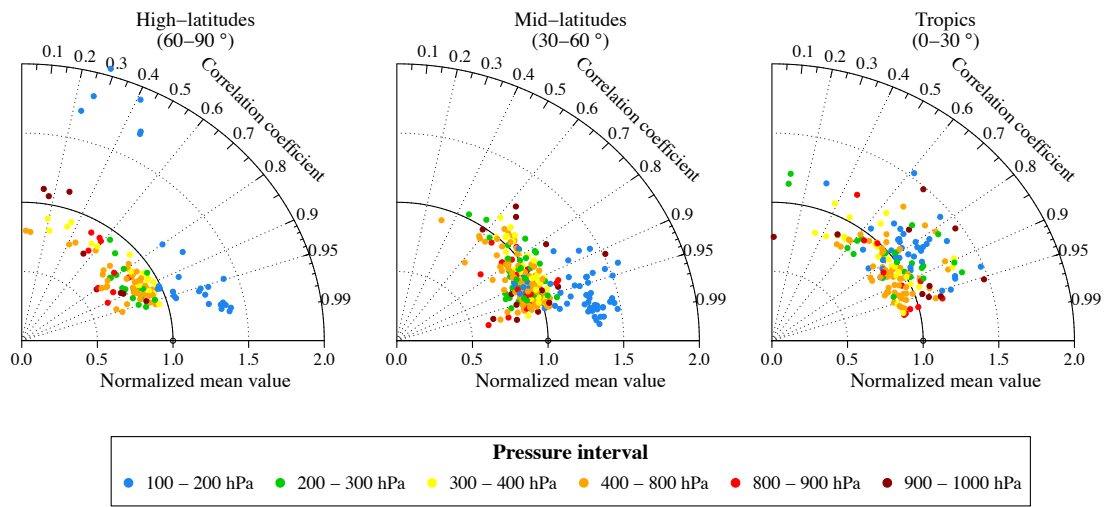


Figure 1. Taylor diagram comparing the mean and temporal correlation of ozone volume mixing ratio between ozonesonde climatology over the 1995-2011 period (Tilmes et al., 2012) and LMDZ-INCA model results, interpolated to the sample locations and vertical levels for high-latitudes (60-90°), mid-latitudes (30-60°) and tropical (0-30°) stations. The colors correspond to different pressure ranges, each including different pressure levels (100-200 hPa: 3 levels; 200-300 hPa: 2 levels; 300-400 hPa: 2 levels; 400-800 hPa: 5 levels; 800-900 hPa: 2 levels; 900-1000 hPa: 2 levels).

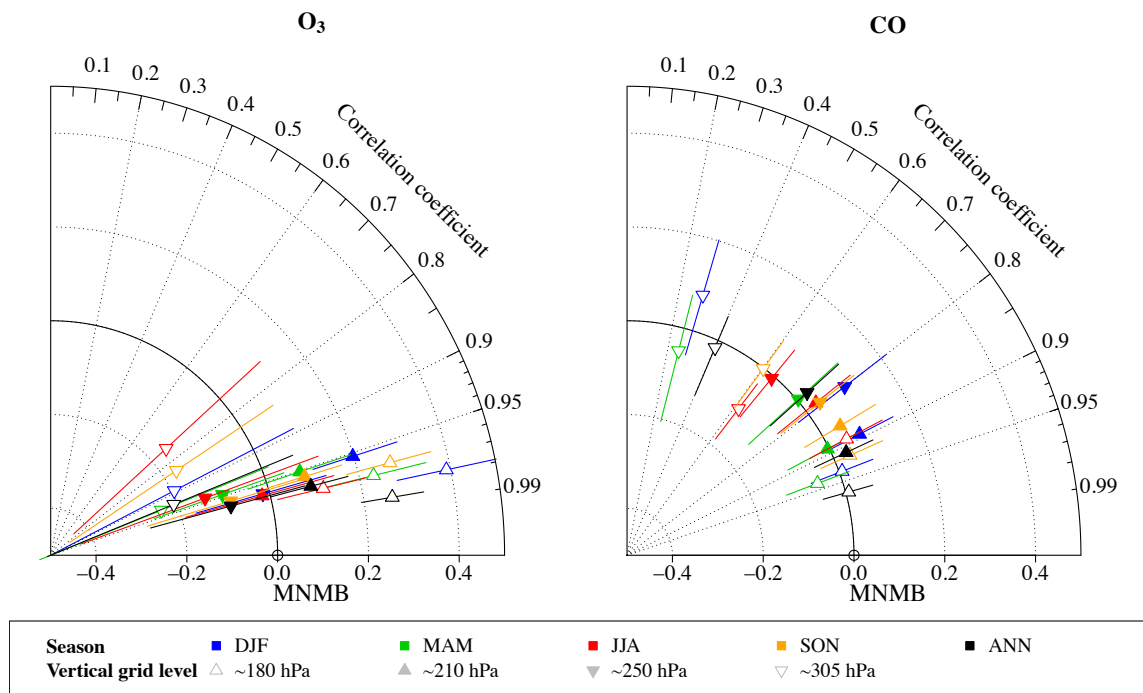


Figure 2. Taylor diagram comparing the mean and geographical correlation of ozone (left) and carbon monoxide (right) volume mixing ratio between the IAGOS data base (Cohen et al., 2018; 2021) and the LMDZ-INCA model results. The error bars denote the 1st and 3rd quartiles of the model to IAGOS biases for a given vertical level and season.

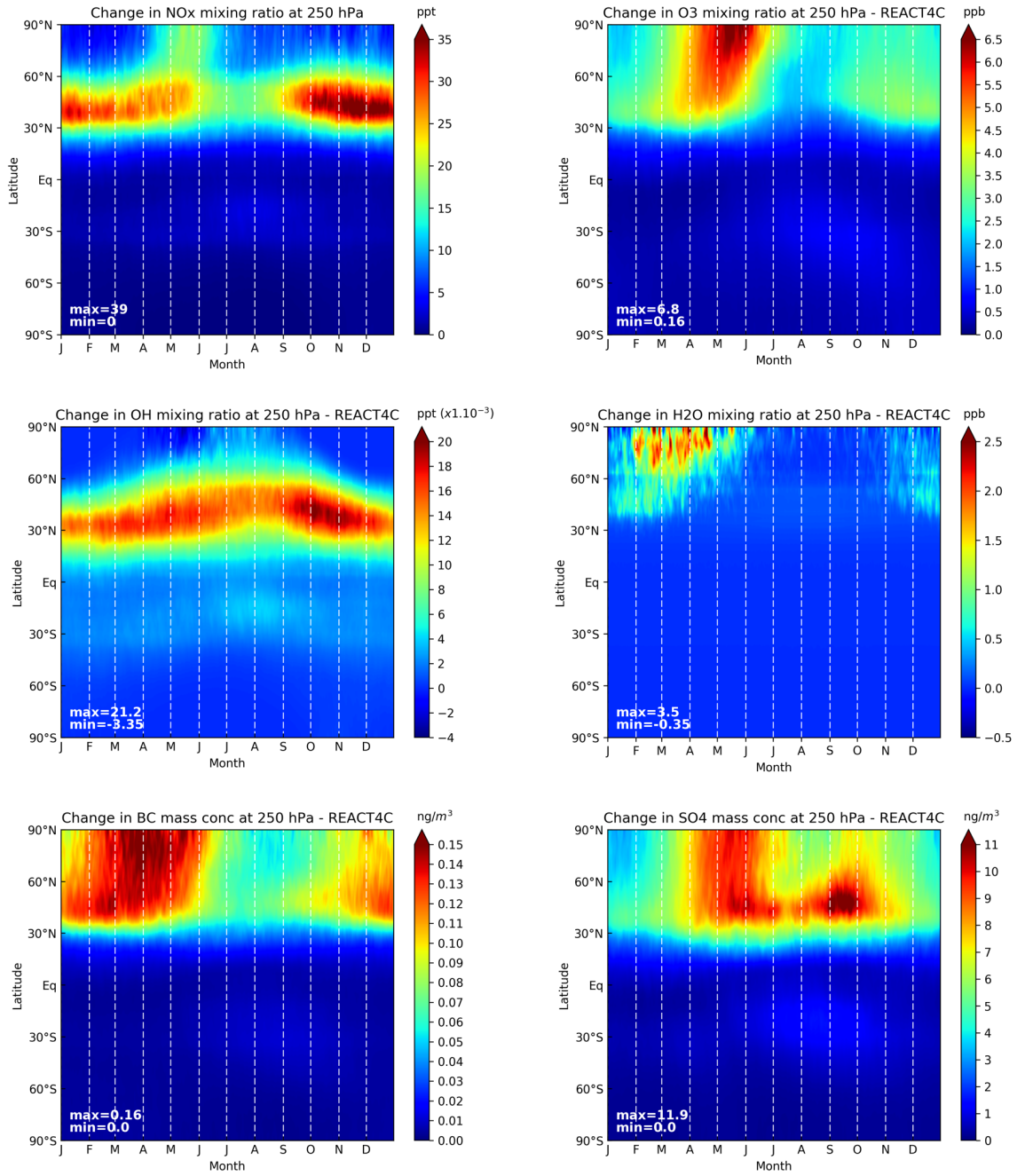


Figure 3. Daily and zonally averaged perturbation due to aircraft emissions at 250 hPa of NO_x (ppt), O₃ (ppbv), OH (10^{-3} pptv), H₂O (ppbv), BC (ng/m³) and SO₄ (ng/m³) for the REACT4C_2006 inventory.

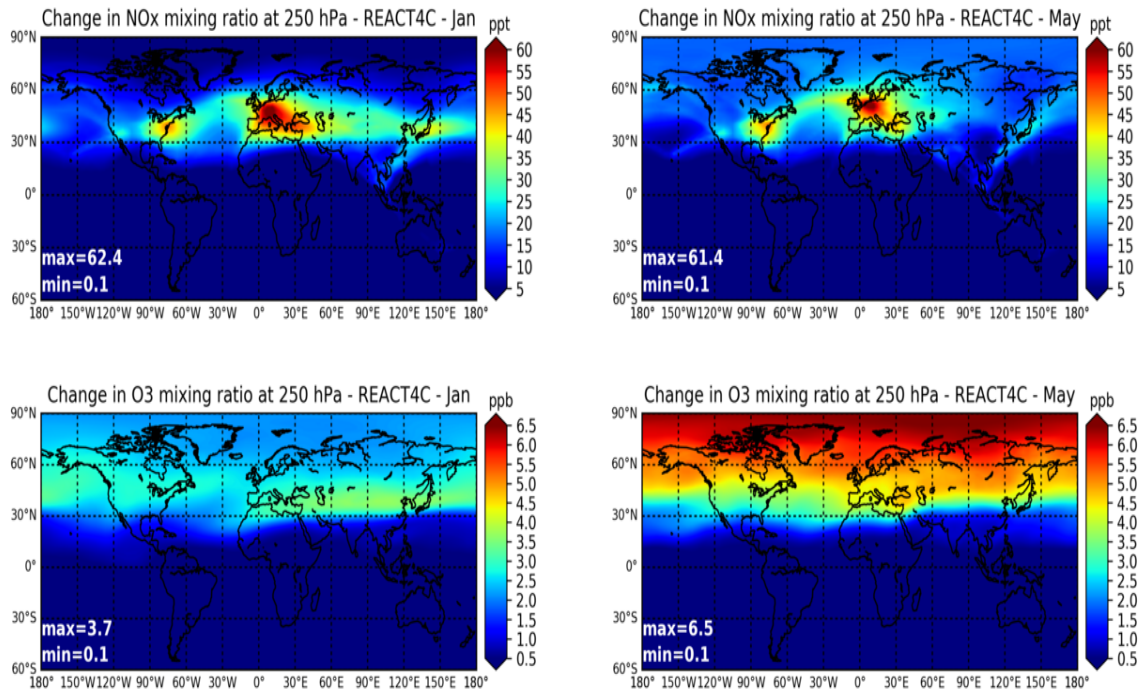


Figure 4. Spatial distribution of the 250 hPa perturbation due to aircraft emissions for the month of January (left) and May (right) for NOx (pptv) and ozone (ppbv) mixing ratio for the REACT4C_2006 inventory.

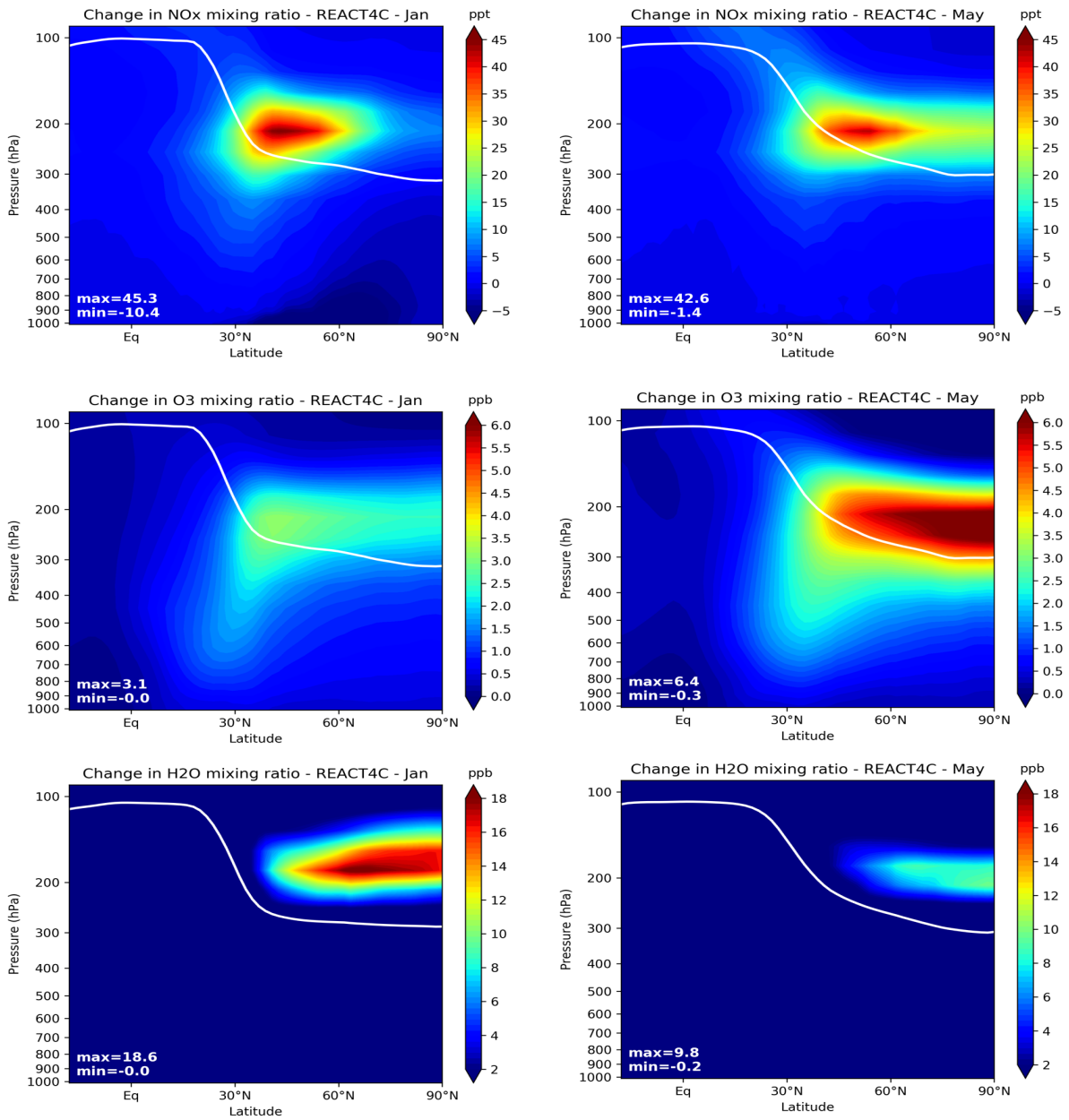


Figure 5. Zonal mean perturbation due to aircraft emissions for January (left) and May (right) of NO_x (pptv), O₃ (ppbv), and H₂O (ppbv) for the REACT4C_2006 inventory. The solid line represents the model tropopause pressure.

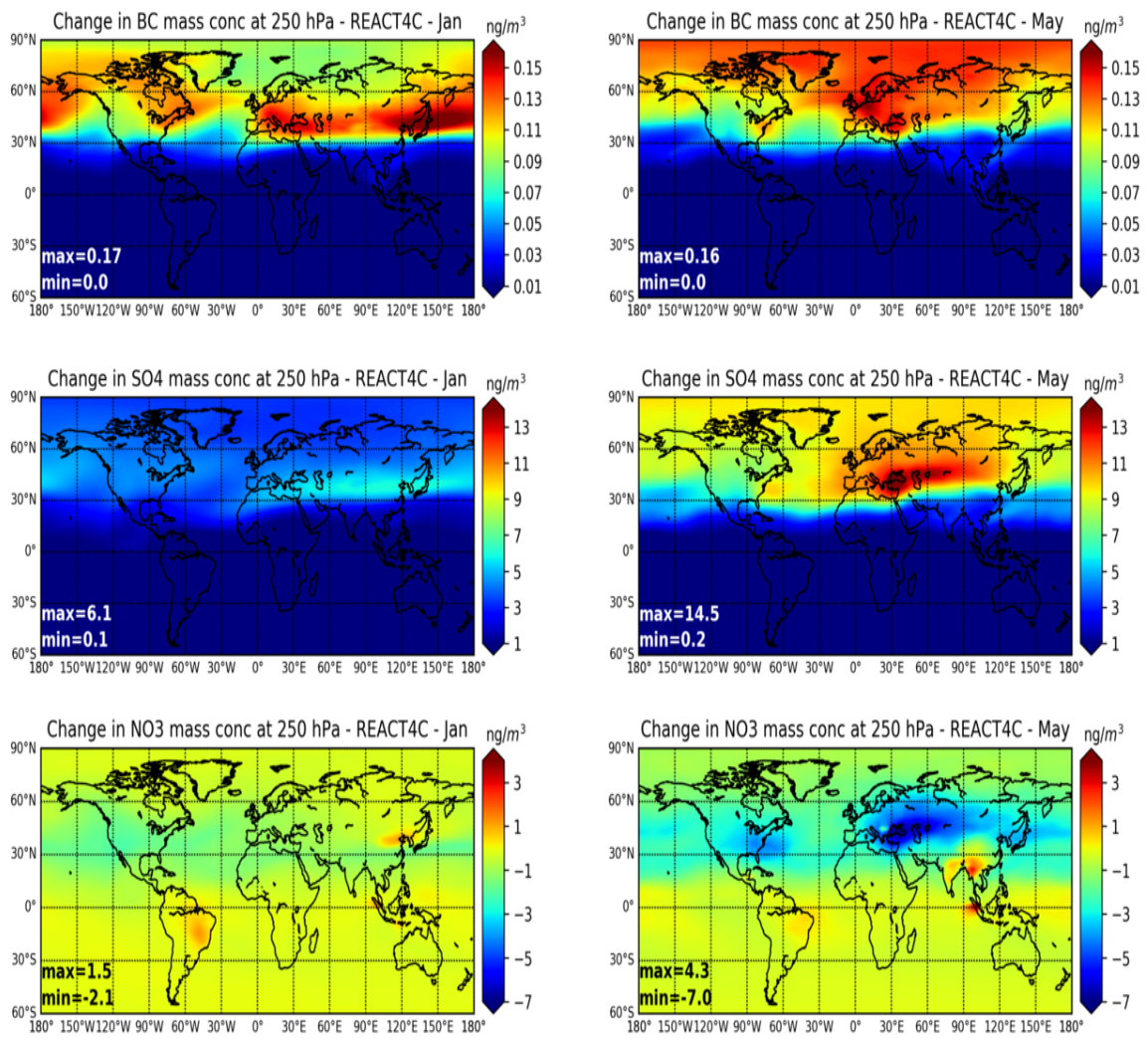


Figure 6. Spatial distributions of the 250 hPa perturbation due to aircraft emissions for January (left) and May (right) for BC, SO₄ and NO₃ (ng/m³) for the REACT4C_2006 inventory.

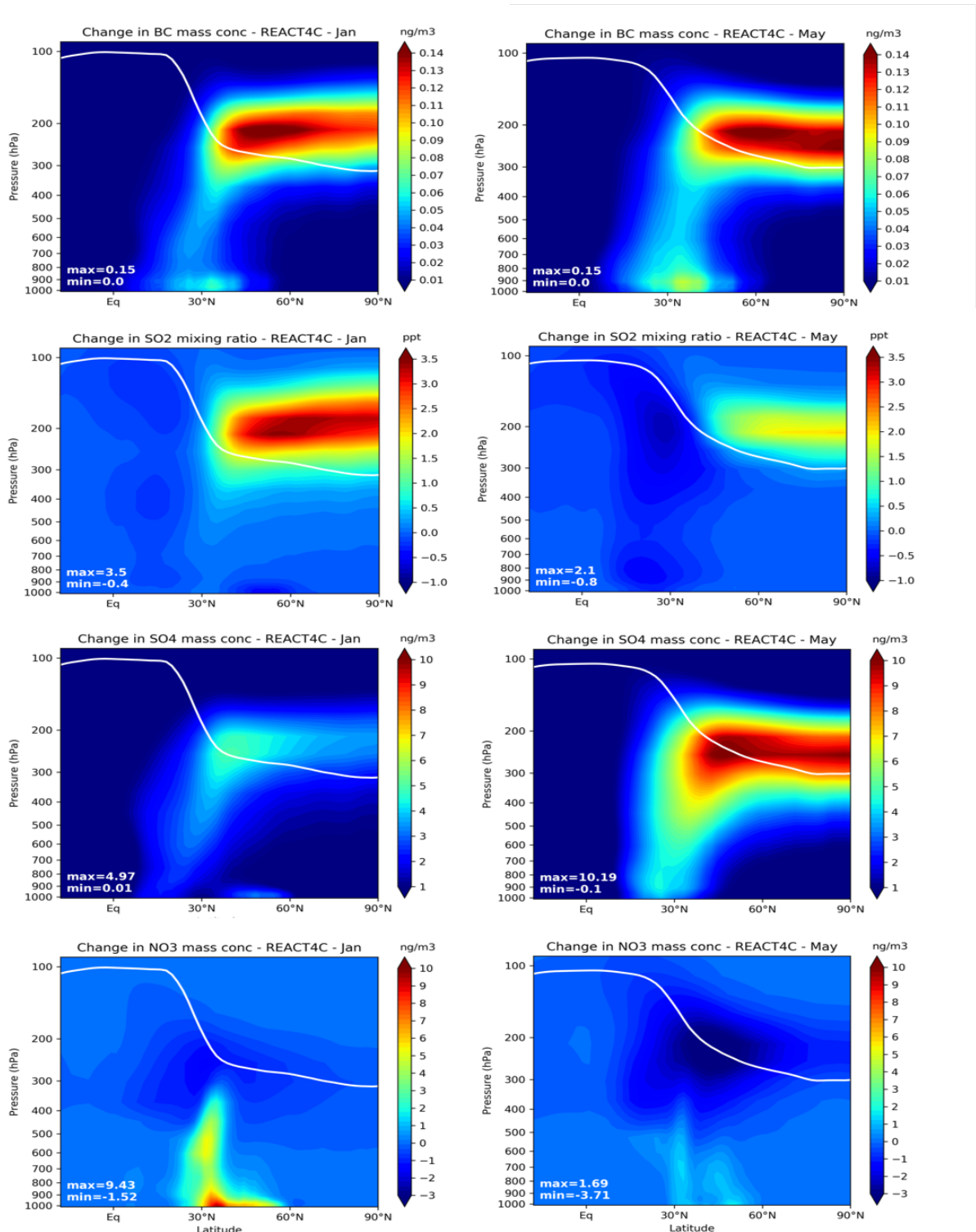


Figure 7. Zonal mean perturbation due to aircraft emissions for January (left) and May (right) of BC (ng/m³), SO₂ (ppt), SO₄ (ng/m³) and NO₃ (ng/m³) for the REACT4C_2006 inventory. The solid line represents the tropopause pressure.

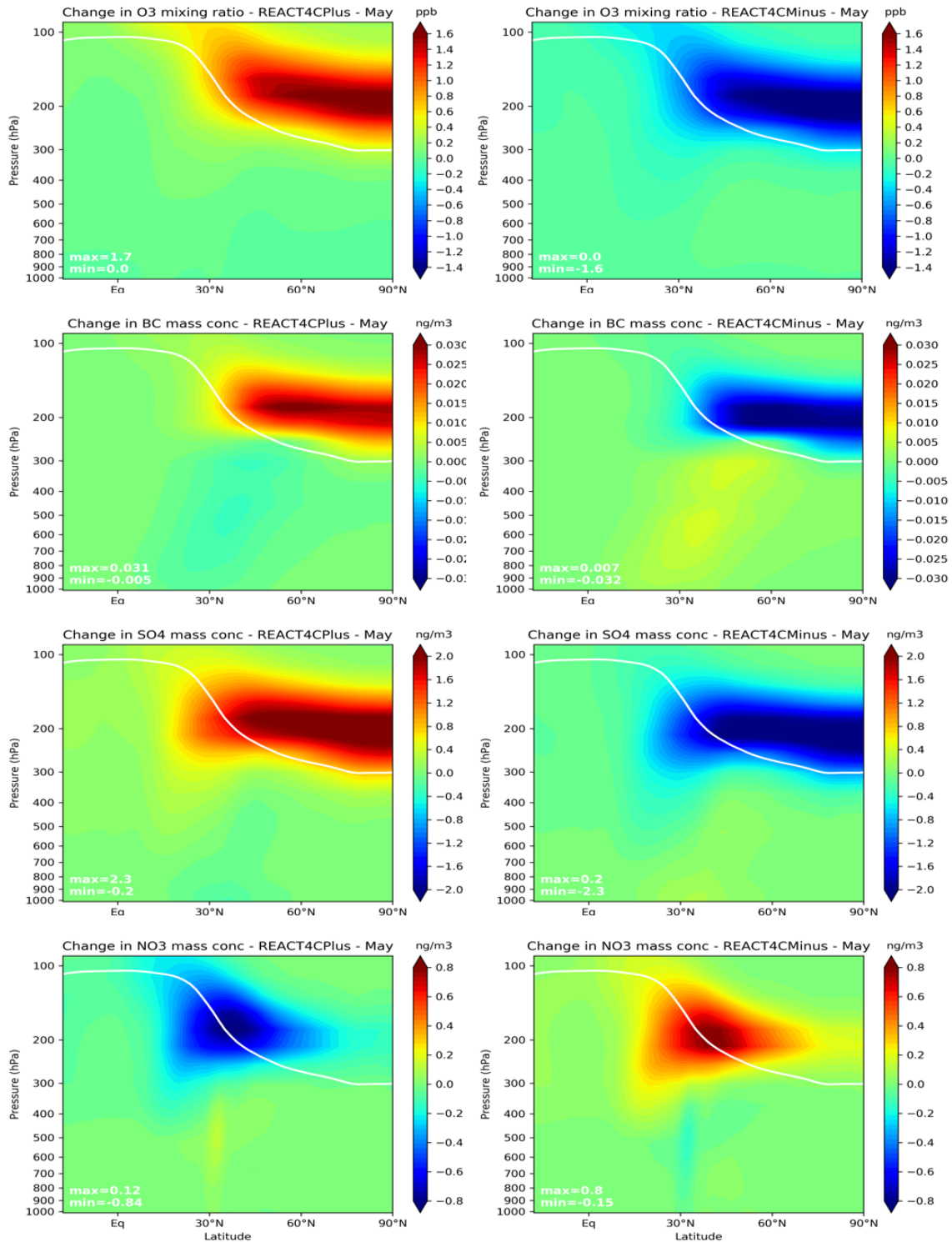


Figure 8. Zonal mean difference for the months of May for O₃ (ppbv), BC (ng/m³), SO₄ (ng/m³) and NO₃ (ng/m³) between the REACT4C_PLUS (left) and REACT4C_MINUS (right) simulations and REACT4C_2006 as the reference. The solid line represents the tropopause pressure.

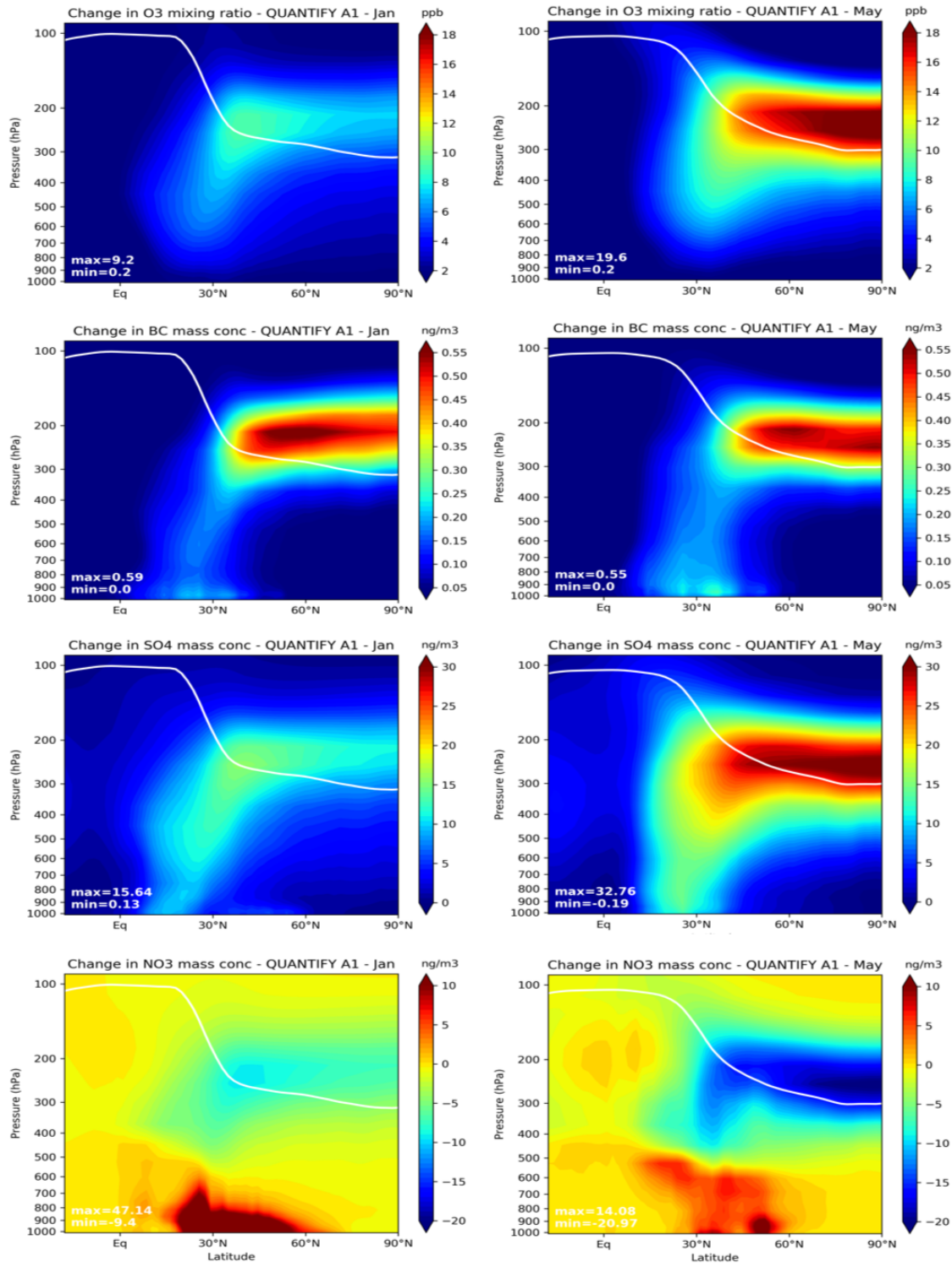


Figure 9. Zonal mean perturbation due to aircraft emissions for the months of January (left) and May (right) for O₃ (ppbv), BC (ng/m³), SO₄ (ng/m³) and NO₃ (ng/m³) averaged for the future scenario QUANTIFY A1 2050. The solid line represents the tropopause pressure.

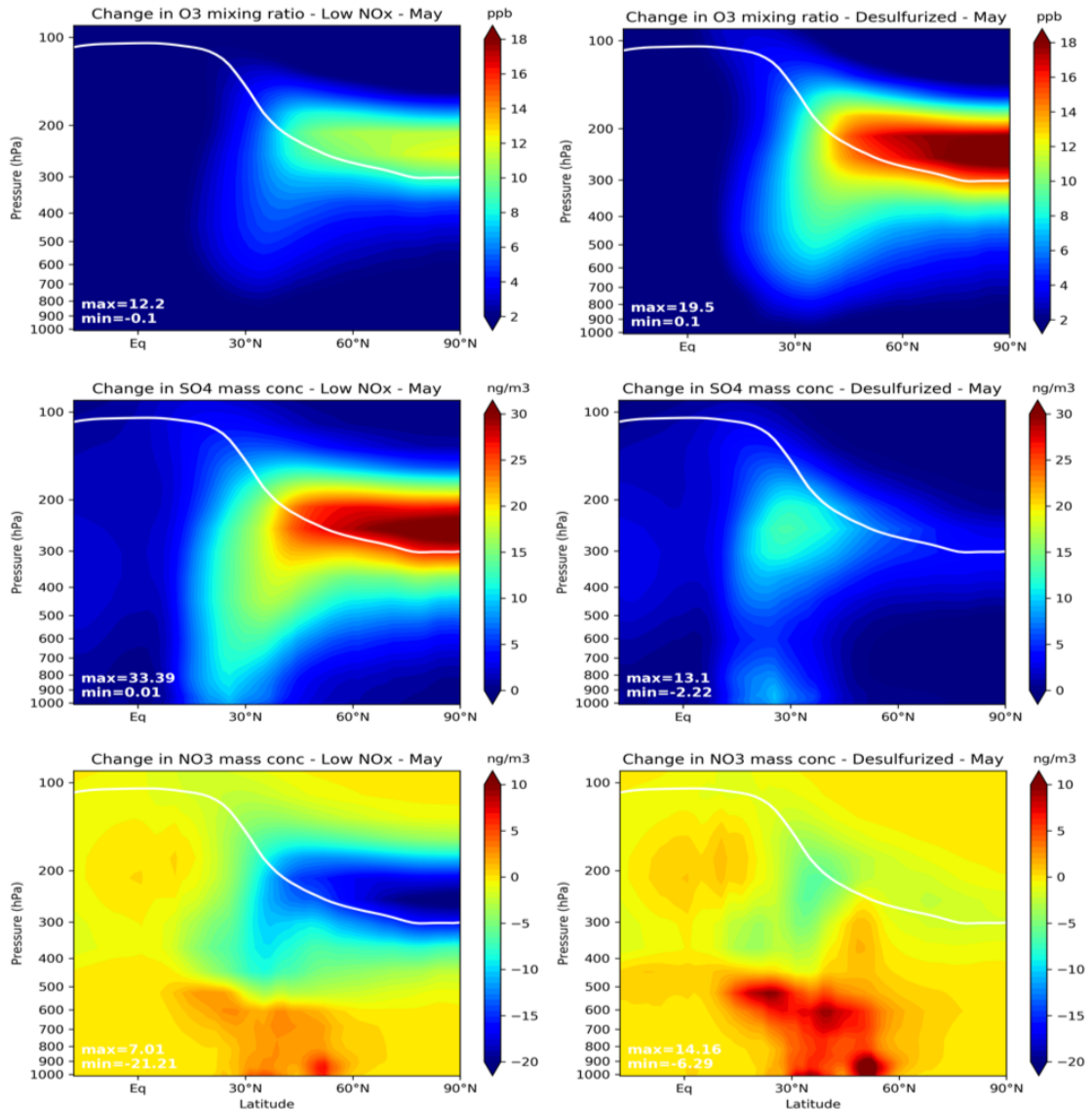


Figure 10. Zonal mean perturbation due to aircraft emissions for May of O₃ (ppbv), SO₄ and NO₃ (ng/m³) for the LowNO_x (left) and Desulfurized (right) scenarios. The solid line represents the tropopause pressure.

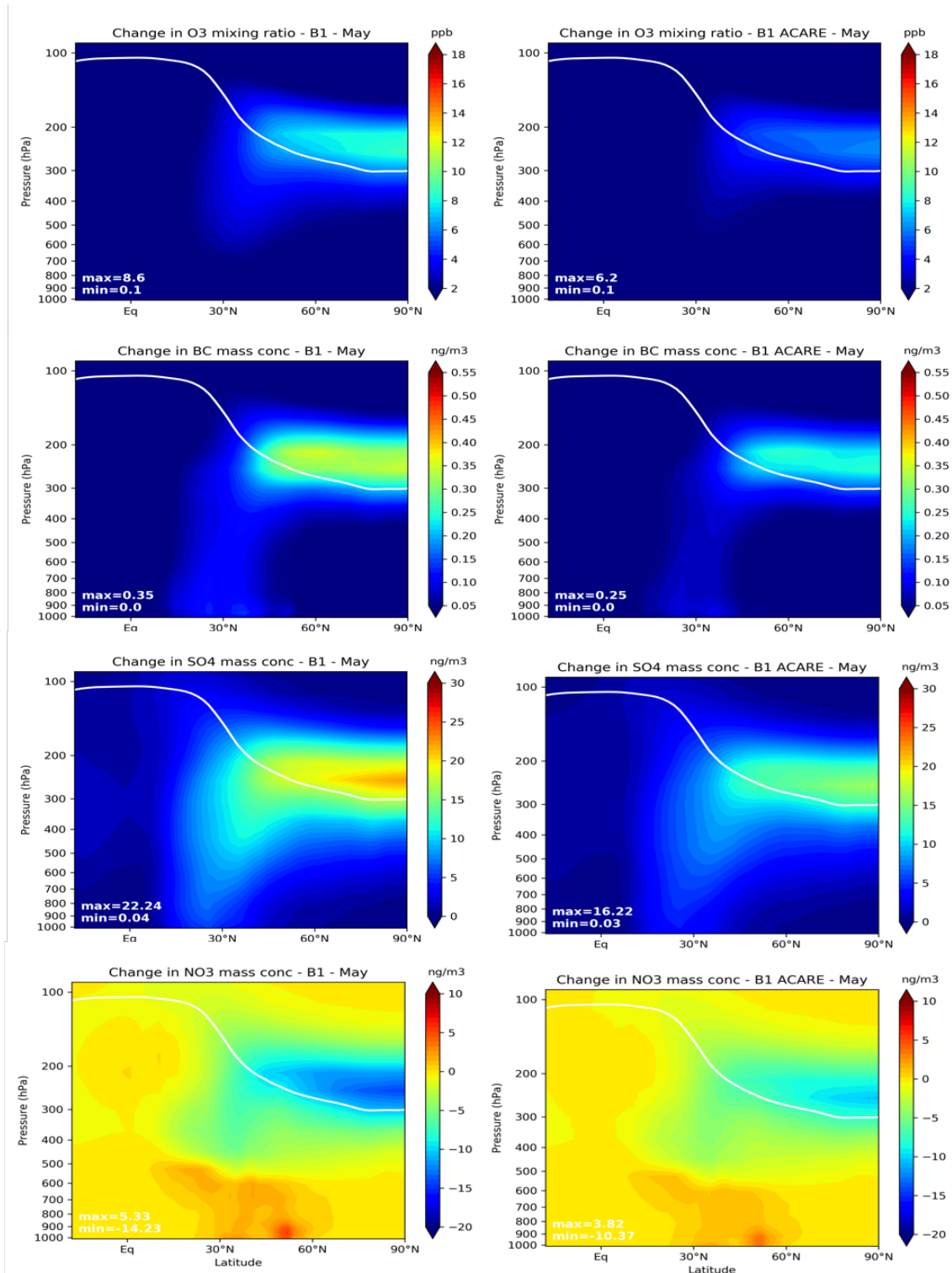


Figure 11. Zonal mean perturbation due to aircraft emissions for May of O_3 (ppbv), BC, SO_4 , and NO_3 (ng/m 3) for the QUANTIFY 2050 B1 (left) and B1 ACARE (right) scenarios. The solid line represents the tropopause pressure.